





CircPVT1 promotes ER-positive breast tumorigenesis and drug resistance by targeting *ESR1* and MAVS

Jia Yi^{1,2,3,†} , Lei Wang^{2,3,†}, Guo-sheng Hu^{2,3}, Yue-ying Zhang^{2,3}, Jiao Du^{2,3}, Jian-cheng Ding^{2,3}, Xiang Ji^{2,3}, Hai-feng Shen^{2,3} , Hai-hua Huang⁴, Feng Ye^{1,*}  & Wen Liu^{2,3,**} 

Abstract

The molecular mechanisms underlying estrogen receptor (ER)-positive breast carcinogenesis and endocrine therapy resistance remain incompletely understood. Here, we report that circPVT1, a circular RNA generated from the lncRNA PVT1, is highly expressed in ER α -positive breast cancer cell lines and tumor samples and is functionally important in promoting ER α -positive breast tumorigenesis and endocrine therapy resistance. CircPVT1 acts as a competing endogenous RNA (ceRNA) to sponge miR-181a-2-3p, promoting the expression of *ESR1* and downstream ER α -target genes and breast cancer cell growth. Furthermore, circPVT1 directly interacts with MAVS protein to disrupt the RIGI–MAVS complex formation, inhibiting type I interferon (IFN) signaling pathway and anti-tumor immunity. Anti-sense oligonucleotide (ASO)-targeting circPVT1 inhibits ER α -positive breast cancer cell and tumor growth, re-sensitizing tamoxifen-resistant ER α -positive breast cancer cells to tamoxifen treatment. Taken together, our data demonstrated that circPVT1 can work through both ceRNA and protein scaffolding mechanisms to promote cancer. Thus, circPVT1 may serve as a diagnostic biomarker and therapeutic target for ER α -positive breast cancer in the clinic.

Keywords anti-tumor immunity; breast cancer; circPVT1; ER α ; MAVS

Subject Categories Cancer; Immunology; RNA Biology

DOI 10.15252/emboj.2022112408 | Received 18 August 2022 | Revised 6 February 2023 | Accepted 2 March 2023 | Published online 3 April 2023

The EMBO Journal (2023) 42: e112408

Introduction

Estrogen receptor (ER)-positive subtype of breast cancer accounts for around 70% of all breast cancer subtypes (Anurag *et al*, 2018; Mesa-Guiagaray *et al*, 2020). One of the important initiating factors is the

disturbance of estrogen (17- β -estradiol, estradiol, E₂), which leads to the abnormal expression of a large number of estrogen/ER-target genes with implication in cell cycle regulation, cell proliferation, and cell metabolism, among others (Anurag *et al*, 2018). ER includes ER α and ER β , which are encoded by *ESR1* and *ESR2* genes, respectively. Treatments that block ER itself and up- or downstream of ER pathways are called endocrine therapies, which are the most important and specific treatments for ER-positive breast cancer. Several classes of endocrine therapy have been developed to date, which include selective ER modulators (SERMs), such as tamoxifen (Osborne, 1998; Clarke *et al*, 2001); aromatase inhibitors (AIs), such as letrozole, anastrozole, and exemestane (Waks & Winer, 2019); and selective ER downregulators (SERDs), such as fulvestrant (ICI; Howell *et al*, 2004; Blackburn *et al*, 2018). However, some ER-positive breast cancer patients do not benefit from endocrine therapy due to primary resistance. Patients with initial benefit may also face difficulties with acquired resistance after prolonged or multi-line endocrine therapy (Shu & Selmanoff, 1991; Rossinnes *et al*, 2011; Pan *et al*, 2017). Evidence suggested that regulatory factors that target ER could facilitate resistance to endocrine therapy (Green & Carroll, 2007). Finding new drug targets and developing novel strategies will bring new hopes for overcoming endocrine therapy resistance of ER-positive breast cancer.

MAVS and STING are two major adapters in the type I interferon (IFN) signaling pathway. MAVS is located in the mitochondria and is responsive to exogenous RNA virus infection or endogenous RNA in cells (Seth *et al*, 2005; Sun *et al*, 2006). STING is located in endoplasmic reticulum and is responsive to exogenous DNA virus infection or endogenous DNA breaks (Ishikawa & Barber, 2008; Ishikawa *et al*, 2009). Upon DNA or RNA stimulation, RLR-MAVS or cGAS-STING can activate TBK1 to phosphorylate IRF3. Phosphorylated IRF3 forms dimer and transfers into the nucleus to bind the promoters and induce the expression of type I IFN and type I IFN-stimulated genes (ISGs) (West *et al*, 2011; Schneider *et al*, 2014; Chen *et al*, 2016; Yum *et al*, 2019; Ablasser & Hur, 2020). Activation

1 Department of Medical Oncology, Xiamen Key Laboratory of Antitumor Drug Transformation Research, The First Affiliated Hospital of Xiamen University, Xiamen, China

2 State Key Laboratory of Cellular Stress Biology, School of Pharmaceutical Sciences, Xiamen University, Xiamen, China

3 Fujian Provincial Key Laboratory of Innovative Drug Target Research, School of Pharmaceutical Sciences, Xiamen University, Xiamen, China

4 Department of Pathology, The Second Affiliated Hospital, Shantou University Medical College, Shantou, China

*Corresponding author. Tel: +86 13860458889; E-mail: yefengdoctor@xmu.edu.cn

**Corresponding author. Tel: +86 18350280846; E-mail: w2liu@xmu.edu.cn

[†]These authors contributed equally to this work

of MAVS and STING plays important roles in anti-tumor immunity (Motwani *et al.*, 2019; Yum *et al.*, 2019; Ablasser & Hur, 2020; Chen & Hur, 2022). It has been reported that low-dose anti-cancer drug decitabine (5-AZA-CdR), a DNA methylation inhibitor, can inhibit colorectal cancer cell growth by inducing viral mimicry. Treatment with 5-AZA-CdR can induce dsRNA expression, mainly from endogenous retroviruses (ERVs), which then activates MAVS-mediated type I IFN pathway (Roulois *et al.*, 2015). Inhibition of LSD1 has also been reported to induce ERVs to activate dsRNA-mediated type I IFN pathway and stimulates anti-tumor immune responses of T cells (Sheng *et al.*, 2018).

Circular RNAs (circRNAs) are highly abundant, conserved, and dynamically expressed in a variety of tissues. Accumulating evidence suggested that circRNAs exert their functions by means of sponging miRNA, contacting with proteins, or translating into proteins (Hansen *et al.*, 2013; Memczak *et al.*, 2013; Ashwal-Fluss *et al.*, 2014; Chen, 2016, 2020; Yang *et al.*, 2017). CircRNAs exhibit differential expression patterns in many diseases, such as cancer. In recent years, increasing number of circRNAs have been shown to be highly associated with many biological processes and diseases (Chen, 2016; Kristensen *et al.*, 2019, 2022; Li *et al.*, 2020). In particular, a number of circRNAs were reported to be associated with immunological pathways. A circular RNA named cia-cGAS is highly expressed in the nucleus of long-term hematopoietic stem cells (LT-HSCs). Cia-cGAS deficiency in mice causes elevated expression of type I IFNs in bone marrow and decreased numbers of dormant LT-HSCs. Under homeostatic conditions, cia-cGAS binds to the DNA sensor cGAS in the nucleus to block its synthase activity (Xia *et al.*, 2018). EBV-encoded circBART2.2 was found to be highly expressed in nasopharyngeal carcinoma, which promotes the transcription of PD-L1 by binding the helicase domain of RIGI and activating downstream IRF3 and NFκB, resulting in tumor immune escape (Ge *et al.*, 2021). CircPVT1 has been reported to play important roles in a variety of diseases (Chen *et al.*, 2017; Zhu *et al.*, 2018; Wang *et al.*, 2020b; Ghafouri-Fard *et al.*, 2021; Palcau *et al.*, 2022). However, whether and how circRNA regulates immune responses

and tumor development in ERα-positive breast cancer remain unknown.

In our previous study, we reported that circPGR, a circRNA induced by estrogen, functions as a miRNA sponge to promote ERα-positive breast cancer cell growth (Wang *et al.*, 2021). We noticed that a number of circRNAs are highly expressed in ERα-positive breast cancer cells. However, whether and how these highly expressed circRNAs function in ERα-positive breast cancer remain unknown. Here, we reported that one of these circRNAs, circPVT1, is highly expressed in ERα-positive breast cancer cell lines and clinical breast tumor samples, which enhances *ESR1* mRNA stability via sponging miR-181a-2-3p, reinforcing the activation of estrogen/ERα-target genes and cell growth. Meanwhile, circPVT1 directly interacts with MAVS to inhibit the formation of RIGI and MAVS complex, suppressing the activation of type I IFN and ISGs and anti-tumor immunity. As expected, targeting circPVT1 inhibits ERα-positive breast cancer cell growth and tumorigenesis and overcomes endocrine therapy resistance.

Results

CircPVT1 is highly expressed in ERα-positive breast cancer cells and is required for ERα-positive breast cancer cell growth and tumorigenesis

We performed circRNA sequencing (circRNA-seq) in an ERα-positive breast cancer cell line, MCF7. There were 25,817, 22,965, and 17,687 circRNAs being predicted from three independent circRNAs algorithms, CIRI2, find_circ, and CIRCexplorer2, respectively (back splicing junction (BSJ) reads ≥ 2). Also, 10,151 circRNAs were found to be predicted in common (Fig 1A). In particular, the top 40 circRNAs with the largest number of BSJ reads identified by these algorithms had 20 in common (Dataset EV1). To identify circRNAs that are required for the growth of ERα-positive breast cancer cells, MCF7 cells were transfected with control siRNA or siRNA specifically

Figure 1. CircPVT1 is highly expressed in ERα-positive breast cancer cells and is required for ERα-positive breast cancer cell growth and tumorigenesis.

- A The overlapping between circRNAs predicted by three different tools, CIRI2, find_circ, and CIRCexplorer2, is shown by Venn diagram (back splicing junction (BSJ) reads ≥ 2).
- B RNA samples extracted from normal breast epithelial cell, MCF10A, and different subtypes of breast cancer cell lines as indicated were subjected to RT-qPCR analysis to examine the expression of circPVT1 ($n = 3$ biological replicates, \pm s.e.m., ns: non-significant, $*P < 0.05$, $**P < 0.01$, $***P < 0.001$ by two-tailed Student's *t*-test).
- C RNA samples extracted from 28 pairs of ER-positive (ER⁺) breast tumor and adjacent normal tissues and 14 pairs of ER-negative (ER⁻) breast tumor and adjacent normal tissues were subjected to RT-qPCR analysis to examine the expression of circPVT1 (\pm s.e.m., $*P < 0.05$, $**P < 0.01$ by two-tailed Student's *t*-test).
- D, E MCF7 cells transfected with control siRNA (si-CTL) or two independent siRNAs specifically targeting circPVT1 (si-circPVT1#1 and si-circPVT1#2) were subjected to RNA extraction and RT-qPCR analysis to examine the expression of circPVT1 (D) and cell proliferation assay (E) ($n = 3$ biological replicates, \pm s.e.m., $***P < 0.001$, day 4 by two-tailed Student's *t*-test for cell proliferation assay).
- F, G MCF7 cells were transfected with control vector or vector expressing circPVT1 followed by RT-qPCR to examine the expression of circPVT1 (F) and cell proliferation assay (G) ($n = 3$ biological replicates, \pm s.e.m., $***P < 0.001$, day 4 by two-tailed Student's *t*-test for cell proliferation assay).
- H, I MCF7 cells were infected with control shRNA (sh-CTL), or two independent shRNAs specifically targeting circPVT1 (sh-circPVT1#1 and sh-circPVT1#2) were subjected to RNA extraction and RT-qPCR analysis to examine the expression of circPVT1 (H) and colony formation assay (I) ($n = 3$ biological replicates, \pm s.e.m., $***P < 0.001$ by two-tailed Student's *t*-test).
- J Quantification of the crystal violet dye as shown in (I) ($n = 3$ biological replicates, \pm s.e.m., $***P < 0.001$ by two-tailed Student's *t*-test).
- K MCF7 cells infected with sh-CTL, sh-circPVT1#1, or sh-circPVT1#2 were injected subcutaneously into female BALB/C nude mice for xenograft experiments.
- L The weight of tumors in (K) is shown ($n = 6$, \pm s.e.m., $**P < 0.01$ by two-tailed Student's *t*-test).
- M 4T1 cells infected with sh-CTL or sh-circPvt1 were injected subcutaneously into female BALB/C mice for allograft experiments.
- N The weight of tumors in (M) is shown ($n = 6$, \pm s.e.m., $**P < 0.01$ by two-tailed Student's *t*-test).
- O Tamoxifen-resistant MCF7 cells transfected with si-CTL, si-circPVT1#1, or si-circPVT1#2 were treated with or without tamoxifen (Tam, 5 μ M, 72 h) followed by cell proliferation assay ($n = 3$ biological replicates, \pm s.e.m., ns: non-significant, $*P < 0.05$, $**P < 0.01$, day 4 by two-tailed Student's *t*-test).

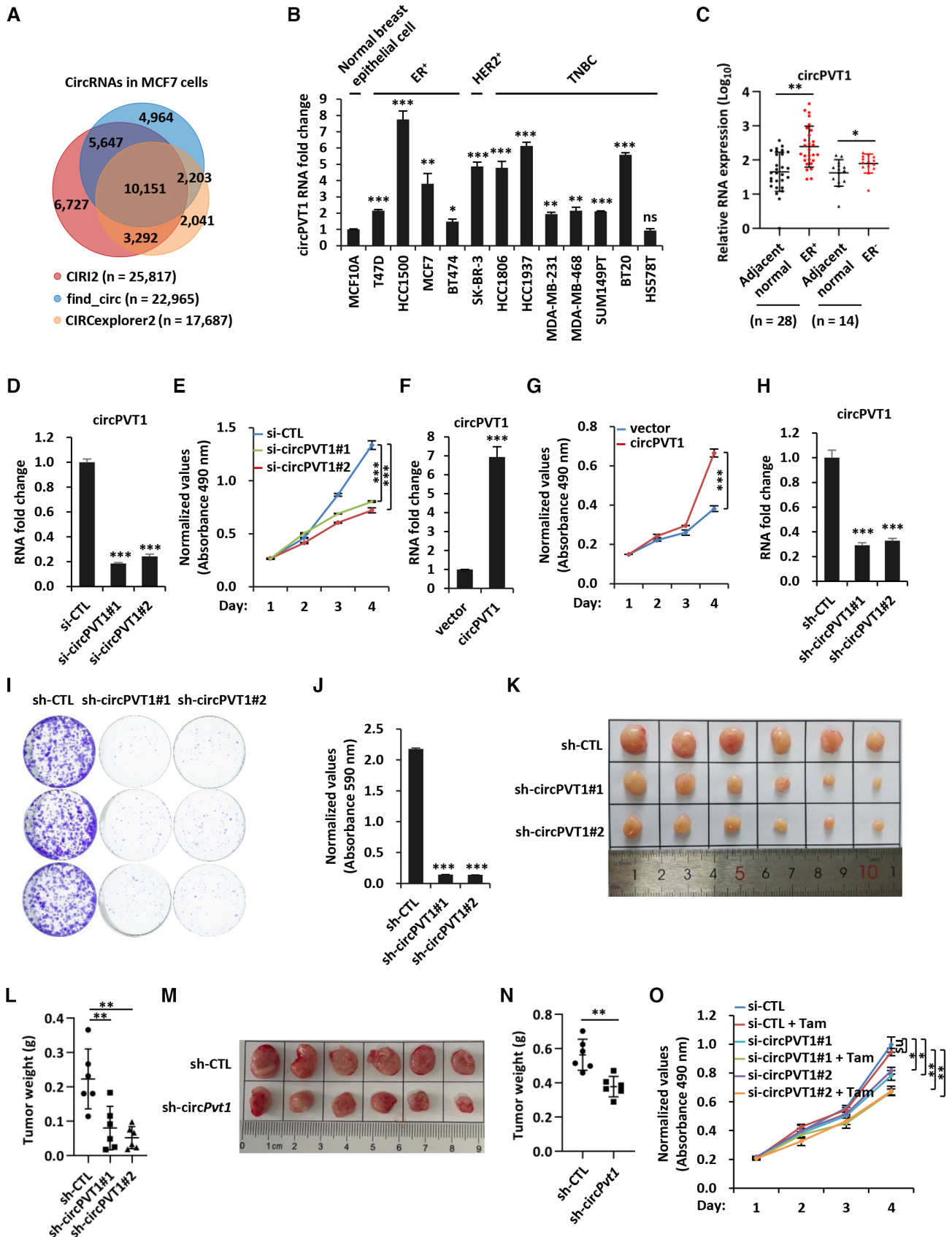


Figure 1.

targeting to eight circRNAs with designable siRNA followed by cell proliferation assay (Fig EV1A–C). It was found that circRNAs including circPVT1, circMIB1, and circCTBP1 were required for the growth of MCF7 cells (Fig EV1C). We focused on studying circPVT1 in the current study. CircPVT1 was found to be highly expressed in breast cancer cells, including ER α -positive, HER2-positive, and triple-negative breast cancer (TNBC) cell lines as well as breast tumor tissues, both ER-positive and ER-negative breast tumor tissues (Fig 1B and C). We, therefore, focused on investigating circPVT1's function in ER α -positive breast cancer in this study.

The requirement of circPVT1 for the growth of MCF7 cells was confirmed by using a second independent siRNA (Fig 1D and E). In contrast, over-expression of circPVT1 promoted MCF7 cell growth (Fig 1F and G). The results from colony formation assay also showed that circPVT1 was required for the growth of MCF7 cells (Fig 1H–J). The requirement of circPVT1 for cell growth was independent confirmed in another ER α -positive breast cancer cell line, T47D (Fig EV1D–J). To further test the effects of circPVT1 on tumor growth *in vivo*, xenograft experiments using MCF7 cells and allograft experiments using 4T1 cells were performed. The results indicated that the knockdown of circPVT1 significantly attenuated tumorigenesis (Fig 1K–N). Endocrine therapy resistance represents one of the major challenges for ER α -positive breast cancer in the clinic. We transfected tamoxifen-resistant-MCF7 cells with control siRNA or two independent siRNAs targeting circPVT1, and then treated cells with or without tamoxifen followed by cell proliferation assay. The results showed that knocking down of circPVT1 could re-sensitize tamoxifen-resistant-MCF7 cells to tamoxifen treatment (Fig 1O). Taken together, our data suggested that circPVT1 promotes ER α -positive breast cancer cell growth both *in vitro* and *in vivo*, and knockdown of circPVT1 overcomes endocrine therapy resistance in ER α -positive breast cancer cells.

CircPVT1 is stably localized in the cytosol of cells

The functional importance of circPVT1 in ER α -positive breast cancer cells prompted us to characterize it in more detail. CircPVT1 originates from the second exon of PVT1, and it is 410 base pairs (bps) in length (Fig 2A). When we digested total RNA extracted from MCF7 cells with RNase R, circPVT1, but not PVT1, exhibited resistance to RNase R digestion (Fig 2B). CircPVT1 was much more stable than PVT1 when MCF7 cells were treated with Actinomycin D (Fig 2C). The results of polysome profiling analysis indicated that circPVT1 was largely associated with ribosome-free fractions, indicating that it is a non-coding RNA (Fig 2D). To serve as a control, ACTIN was found to be associated with polysome fractions (Fig 2E). Next, cellular fractionation followed by RNA extraction and RT-qPCR analysis indicated that circPVT1 was predominantly localized in the cytosol of cells, which was consistent with the fact that most of the exonic circRNAs are cytosolic (Fig 2F). RNA-FISH analysis results confirmed the cytosolic localization of circPVT1 (Fig 2G). Taken together, our data indicated that circPVT1 is an exonic circRNA and stably localized in the cytosol of cells.

CircPVT1 is required for the expression of estrogen/ER α -target genes

The functional important of circPVT1 in breast tumorigenesis and drug resistance prompted us to identify target genes regulated by

circPVT1. To this end, RNA-seq analysis was performed by knocking down circPVT1 in MCF7 cells. The impact of both siRNAs targeting circPVT1 on the whole transcriptome is well correlated (Pearson correlation coefficient = 0.615) (Fig 3A). There were 853 and 1,126 genes positively and negatively regulated by circPVT1, respectively (Fig 3B). The results of hallmark gene sets analysis for genes positively regulated by circPVT1 revealed that “Estrogen Response Early” and “Estrogen Response Late” were the top two most enriched terms (Fig 3C). These genes are well known to be implicated in cell proliferation, metastasis, metabolism, and endocrine therapy resistance. CircPVT1's effects on representative estrogen/ER α -target genes from RNA-seq were shown (Fig 3D and E), which were further confirmed by RT-qPCR analysis in both MCF7 (Fig 3F and G) and T47D cells (Fig EV2A). To support the functional importance of these circPVT1-regulated estrogen/ER α -target genes in tumor development, the expression of representative ones, such as *TFPI1*, *PGR*, and *GREB1*, was found to be significantly inhibited when circPVT1 was knocked down in MCF7 cell-derived xenografts (Figs 1K and 3H). Taken together, our data suggested that circPVT1 activates estrogen/ER α -target genes to promote ER α -positive breast tumorigenesis.

CircPVT1 acts as a ceRNA to sponge miR-181a-2-3p to modulate *ESR1* mRNA stability and downstream estrogen/ER α -target genes

To investigate how circPVT1 regulates estrogen/ER α -target genes, we sought to construct the competing endogenous RNA (ceRNA) network. To this end, RegRNA2.0 (Chang *et al*, 2013), miRanda (Betel *et al*, 2008), RNAhybrid (Rehmsmeier *et al*, 2004), and TarPmiR (Ding *et al*, 2016) were used to predict potential miRNAs that can bind to circPVT1 at high stringency. CeRNA network construction led to 16 circPVT1-miRNA-mRNA (gene positively regulated by circPVT1) hubs (Fig EV2B). Three hubs caught our attention due to that one of the mRNA targets in these hubs was *ESR1*, the master regulator of estrogen-induced gene transcription (Fig EV2B). Specifically, miR-181a-2-3p, miR-449b-3p, and miR-6715b-5p were predicted to target to both the 3' untranslated region (UTR) of *ESR1* and circPVT1 (Figs 4A and EV2B–D). We first validated that the levels of *ESR1* mRNA and its protein product ER α were dramatically decreased after knocking down of circPVT1 (Figs 4B–D and EV2E and F). Importantly, *ESR1* decreased dramatically in circPVT1-knockdown, MCF7 cell-derived xenografts (Figs 1K and 4E).

The results of RNA immunoprecipitation (RIP) analysis showed that circPVT1 was successfully pulled down by AGO2 (Fig 4F), suggesting that circPVT1 has the potential to bind with miRNAs. We then examined whether miR-181a-2-3p, miR-449b-3p, and miR-6715b-5p can bind to circPVT1. The luciferase activity of circPVT1 (WT)-*luc* was significantly inhibited by both miR-181a-2-3p and miR-6715b-5p, but not miR-449b-3p (Figs 4G and EV2C). To support that miR-181a-2-3p and miR-6715b-5p binding to the predict sites in circPVT1, luciferase reporter constructs with the miR-181a-2-3p or miR-6715b-5p binding site mutated (circPVT1 (MT)-*luc*) were no longer responsive to mimic transfection (Figs 4H and EV2C). Furthermore, circPVT1, miR-181a-2-3p, and miR-6715b-5p were specifically pulled down by the anti-sense oligonucleotide targeting circPVT1, but not the sense one (Fig 4I).

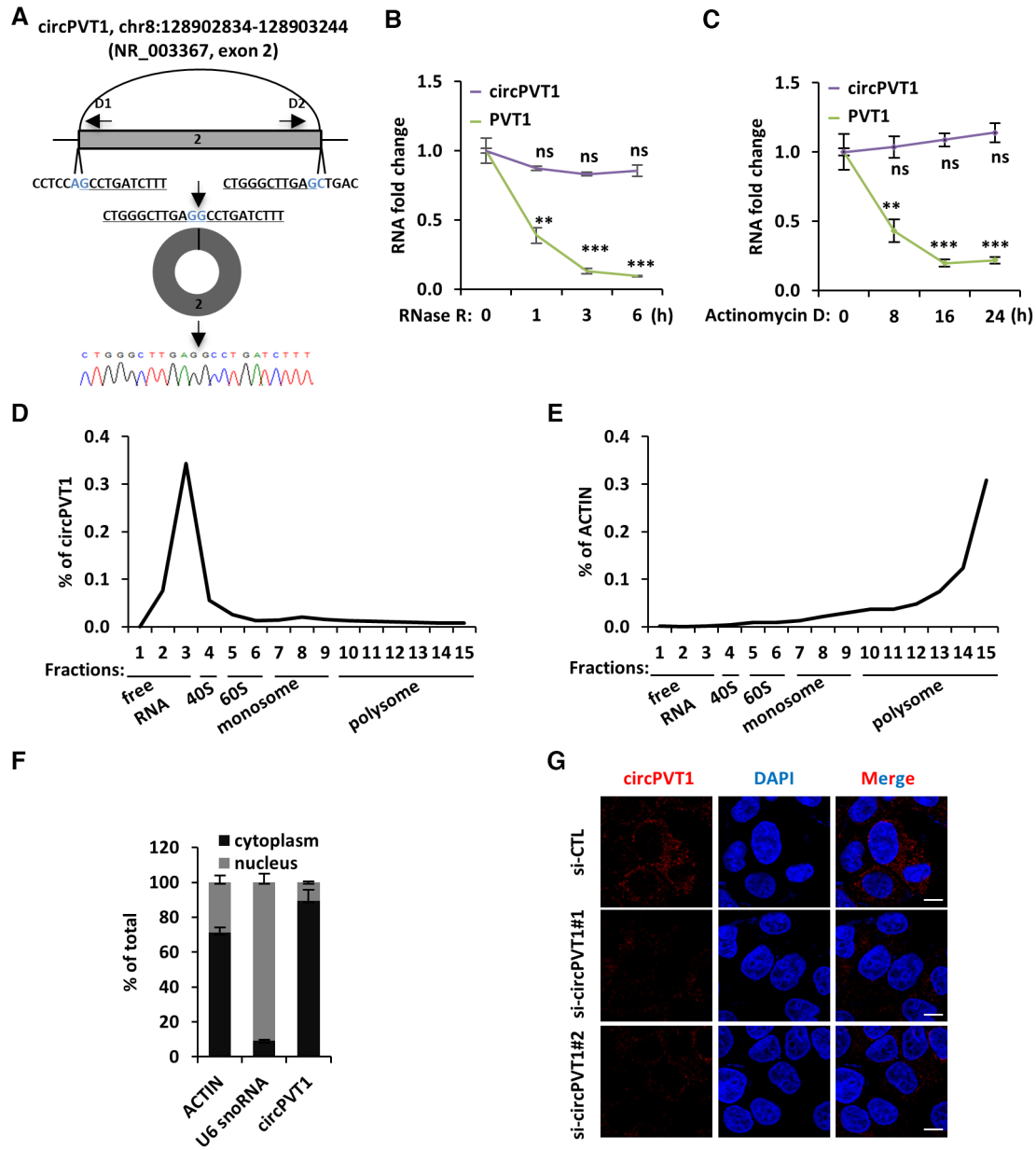


Figure 2. CircPVT1 is stably localized in the cytosol of cells.

- A** RNA sample from MCF7 cells was subjected to reverse transcription, and standard PCR was performed by using divergent primer sets flanking the junction region of circPVT1, followed by Sanger sequencing. Sequence flanking junction region is shown. Junction site is highlighted in light blue. Sanger sequencing histogram is shown at the bottom. D1: divergent primer 1; D2: divergent primer 2.
- B** Total RNAs extracted from MCF7 cells were incubated with or without RNase R (10 units/ μ g RNA) at 37°C for duration as indicated, followed by RT-qPCR analysis to examine the expression of PVT1 or circPVT1 ($n = 3$ biological replicates, \pm s.e.m., ns: non-significant, $**P < 0.01$, $***P < 0.001$ by two-tailed Student's t -test).
- C** MCF7 cells were treated with Actinomycin D (10 g/ml) for duration as indicated, followed by RT-qPCR analysis to examine the expression of PVT1 or circPVT1 ($n = 3$ biological replicates, \pm s.e.m., ns: non-significant, $**P < 0.01$, $***P < 0.001$ by two-tailed Student's t -test).
- D, E** MCF7 cells were subjected to polysome profiling assay, and the resultant fractions were subjected to RNA extraction and RT-qPCR analysis to examine the expression of circPVT1 (D) and ACTIN (E). Fractions 1–3: free RNA (unbound with ribosome); Fraction 4: 40S (40S ribosomal subunit); Fractions 5 and 6: 60S (60S ribosomal subunit); Fractions 7–9: monosome; Fractions 10–15: polysome.
- F** MCF7 cells were subjected to cellular fractionation followed by RNA extraction and RT-qPCR analysis to quantify the amount of circRNA in both nucleus and cytosol of the cells. ACTIN and U6 snoRNA were served as purity control for cytosolic and nuclear fractions, respectively ($n = 3$ biological replicates, \pm s.e.m.).
- G** MCF7 cells transfected with si-CTL, si-circPVT1#1, or si-circPVT1#2 were subjected to RNA-FISH analysis using probe specifically targeting circPVT1. Red: circPVT1; Blue: DAPI. Scale bar, 5 μ m.

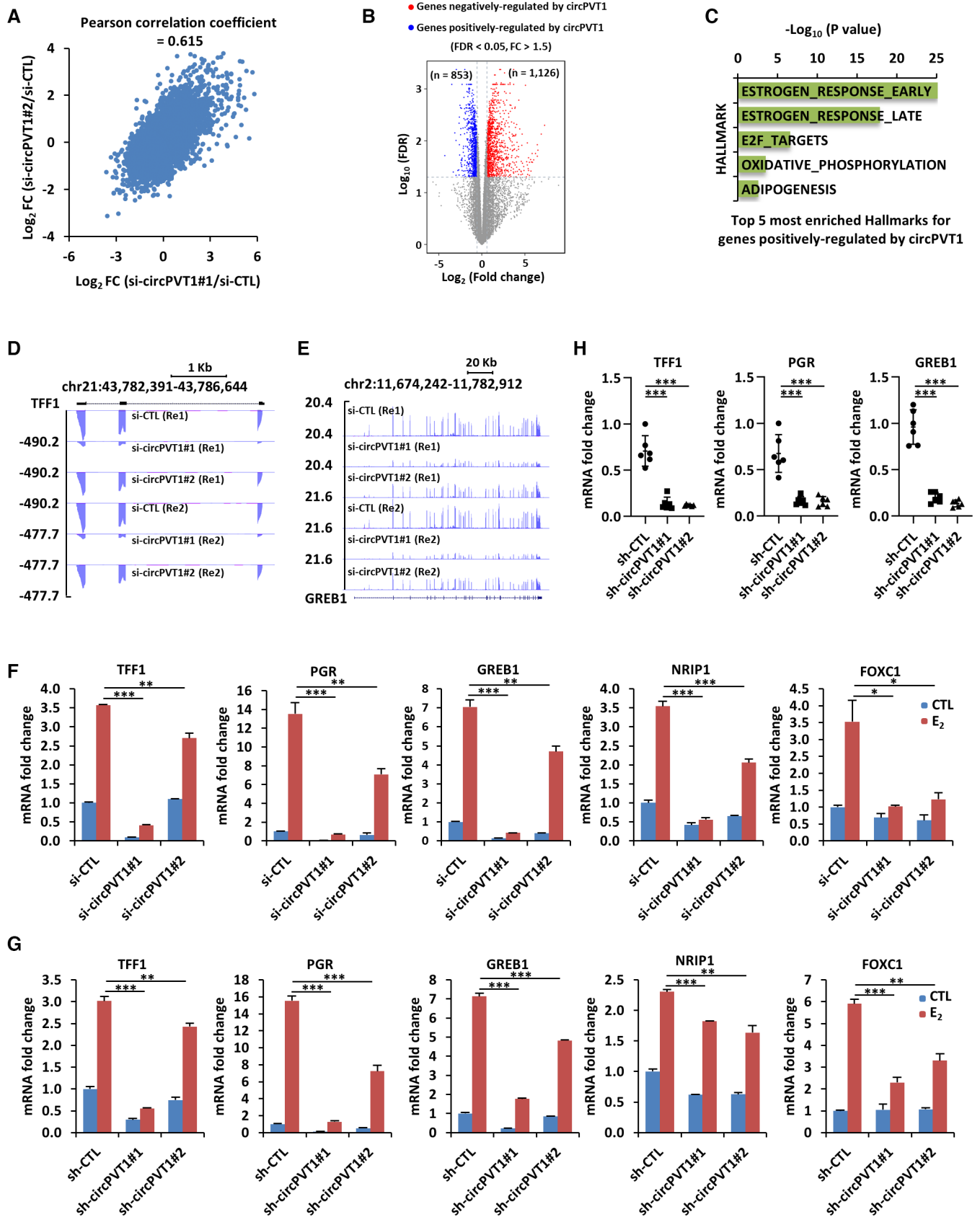


Figure 3.

Figure 3. CircPVT1 is required for the expression of estrogen/ER α -target genes.

- A, B MCF7 cells were transfected with control siRNA (si-CTL) or two individual siRNAs specific against circPVT1 (si-circPVT1#1 and si-circPVT1#2) followed by RNA-seq. The correlation between the effects of the two si-circPVT1s on the whole transcriptome is shown (Pearson correlation coefficient = 0.615) (A). Genes that are positively and negatively regulated by circPVT1 are shown by volcano plot (FDR < 0.05, FC > 1.5) (B).
- C The five most enriched hallmark terms for genes positively regulated by circPVT1 are shown.
- D, E UCSC genome browser views of RNA-seq as described in (A) for *TFE1* (D) and *GREB1* (E) are shown.
- F MCF7 cells transfected with si-CTL, si-circPVT1#1, or si-circPVT1#2 were treated with or without estrogen (E_2 , 10^{-7} M, 6 h) followed by RNA extraction and RT-qPCR analysis to examine the expression of genes as indicated ($n = 3$ biological replicates, \pm s.e.m., * $P < 0.05$, ** $P < 0.01$, *** $P < 0.001$ by two-tailed Student's t -test).
- G MCF7 cells infected with sh-CTL, sh-circPVT1#1, or sh-circPVT1#2 were treated with or without estrogen (E_2 , 10^{-7} M, 6 h) followed by RNA extraction and RT-qPCR analysis to examine the expression of genes as indicated ($n = 3$ biological replicates, \pm s.e.m., ** $P < 0.01$, *** $P < 0.001$ by two-tailed Student's t -test).
- H Tumor samples as described in Fig 1K were subjected to RNA extraction and RT-qPCR analysis to examine the expression of genes as indicated ($n = 6$ biological replicates, \pm s.e.m., *** $P < 0.001$ by two-tailed Student's t -test).

We next tested whether miR-181a-2-3p and miR-6715b-5p regulate the expression of *ESR1*, the target for circPVT1. The luciferase activity of *ESR1* 3' UTR (WT)-*luc*, but not *ESR1* 3' UTR (MT)-*luc*, was significantly inhibited by both miR-181a-2-3p and miR-6715b-5p, confirming that they bind to the predicted sites in the 3' UTR of *ESR1* (Figs 4J and EV2D). The molecular basis for circPVT1 to function as a ceRNA to sponge miRNAs is that the copy number of these molecules is comparable. The results of the copy number analysis revealed that the copy number of circPVT1 and miR-181a-2-3p was comparable, while that for miR-6715b-5p was too few (Figs 4K and EV2G). We then focused on whether circPVT1 works through miR-181a-2-3p to regulate the expression of *ESR1*, estrogen/ER α -target genes, and breast cancer cell growth. As expected, miR-181a-2-3p inhibitor could rescue the decreased expression of *ESR1* at both mRNA and protein levels as well as estrogen/ER α -target genes (Fig 4L–N). The reduced expression of *ESR1* caused by miR-181a-2-3p mimic transfection was

reversed by circPVT1 (WT), but not circPVT1 (MT) with the miR-181a-2-3p binding site mutated, further supporting that circPVT1 regulation of *ESR1* is dependent on miR-181a-2-3p binding (Fig EV2H). Furthermore, circPVT1-regulated breast cancer cell growth was also found to be dependent on miR-181a-2-3p (Fig 4O–Q). The miR-181a-2-3p inhibitor alone exhibited no apparent effects on the expression of *ESR1* and estrogen/ER α -target genes as well as MCF7 cell growth (Fig EV2I and J), which might be because the copy number of miR-181a-2-3p is relatively low, at least lower than that of circPVT1 in MCF7 cells, and the amount of free miR-181a-2-3p is limited (Figs 4K and EV2G). However, the expression of *ESR1* and estrogen/ER α -target genes was decreased, and MCF7 cell growth was inhibited upon miR-181a-2-3p mimic transfection (Fig EV2K and L). Taken together, circPVT1 activates estrogen/ER α -target genes and promotes ER α -positive breast cancer cell growth by stabilizing *ESR1* expression through sponging miR-181a-2-3p.

Figure 4. CircPVT1 acts as a ceRNA to sponge miR-181a-2-3p to stabilize *ESR1* mRNA and downstream estrogen/ER α -target genes.

- A The three miRNAs, miR-449b-3p, miR-181a-2-3p, and miR-6715b-5p that can bind to both circPVT1 and *ESR1* predicted by ceRNA network analysis are shown.
- B UCSC genome browser views of RNA-seq as described in Fig 3A for *ESR1* are shown.
- C, D MCF7 cells transfected with control siRNA (si-CTL) or siRNAs specifically targeting circPVT1 (si-circPVT1#1 and si-circPVT1#2) were treated with or without estrogen (E_2 , 10^{-7} M, 6 h) followed by RT-qPCR analysis (C) and immunoblotting analysis (D) to examine the expression of ER α ($n = 3$ biological replicates, \pm s.e.m., ** $P < 0.01$, *** $P < 0.001$ by two-tailed Student's t -test).
- E Tumor samples as described in Fig 1K were subjected to RNA extraction and RT-qPCR analysis to examine the expression of *ESR1* ($n = 6$ biological replicates, \pm s.e.m., *** $P < 0.001$ by two-tailed Student's t -test).
- F RNA immunoprecipitation (RIP) was performed in MCF7 cells by using control IgG or anti-AGO2 antibody followed by RT-qPCR analysis to examine the binding of circPVT1 and U6 snoRNA ($n = 3$ biological replicates, \pm s.e.m., ns: non-significant, *** $P < 0.001$ by two-tailed Student's t -test).
- G Full-length, linear sequence of circPVT1 was cloned into psiCHECK2 luciferase reporter vector (circPVT1-*luc*), which were then transfected into HEK293T cells with control (CTL), miR-181a-2-3p, miR-449b-3p, or miR-6715b-5p mimic followed by luciferase activity measurement ($n = 3$ biological replicates, \pm s.e.m., * $P < 0.05$ by two-tailed Student's t -test).
- H Wild-type circPVT1-*luc* (circPVT1 (WT)-*luc*) and its mutant form with the potential miR-181a-2-3p or miR-6715b-5p binding site mutated (circPVT1 (MT)-*luc*) were transfected into HEK293T cells with or without CTL, miR-181a-2-3p, or miR-6715b-5p mimic followed by luciferase activity measurement ($n = 3$ biological replicates, \pm s.e.m., ns: non-significant, ** $P < 0.01$ by two-tailed Student's t -test).
- I Oligonucleotide pull-down assay was performed by incubating MCF7 cell lysates with sense or anti-sense oligonucleotide-targeting circPVT1 followed by RT-qPCR analysis to detect the associated RNA as indicated ($n = 3$ biological replicates, \pm s.e.m., ns: non-significant, * $P < 0.05$, *** $P < 0.001$ by two-tailed Student's t -test).
- J The 3' untranslated region (UTR) of *ESR1* (*ESR1* (WT)-*luc*) and its mutant form with the miR-181a-2-3p or miR-6715b-5p binding site mutated (*ESR1* (MT)-*luc*) were cloned into psiCHECK2 luciferase reporter vector, which were then transfected with or without CTL, miR-181a-2-3p, or miR-6715b-5p mimic into HEK293T cells followed by luciferase activity measurement ($n = 3$ biological replicates, \pm s.e.m., ns: non-significant, *** $P < 0.001$ by two-tailed Student's t -test).
- K MCF7 cells were subjected to copy number analysis for genes as indicated. Copy number was calculated based on the standard curves as shown in Fig EV3G.
- L–N MCF7 cells transfected with si-CTL or si-circPVT1 in the presence or absence of miR-181a-2-3p inhibitor were subjected to RT-qPCR analysis (L, N) to examine the expression of genes as indicated and immunoblotting analysis (M) using antibodies as indicated ($n = 3$ biological replicates, \pm s.e.m., ** $P < 0.01$, *** $P < 0.001$ by two-tailed Student's t -test).
- O MCF7 cells transfected with si-CTL or si-circPVT1 in the presence or absence of miR-181a-2-3p inhibitor were subjected to cell proliferation assay ($n = 3$ biological replicates, \pm s.e.m., ns: non-significant, ** $P < 0.01$, day 4 by two-tailed Student's t -test).
- P MCF7 cells that were infected with control shRNA (sh-CTL) or shRNAs specifically targeting circPVT1 (sh-circPVT1) in the presence or absence of miR-181a-2-3p inhibitor were subjected to colony formation assay.
- Q Quantification of the crystal violet dye as shown in (P) ($n = 3$ biological replicates, \pm s.e.m., ** $P < 0.01$ by two-tailed Student's t -test).

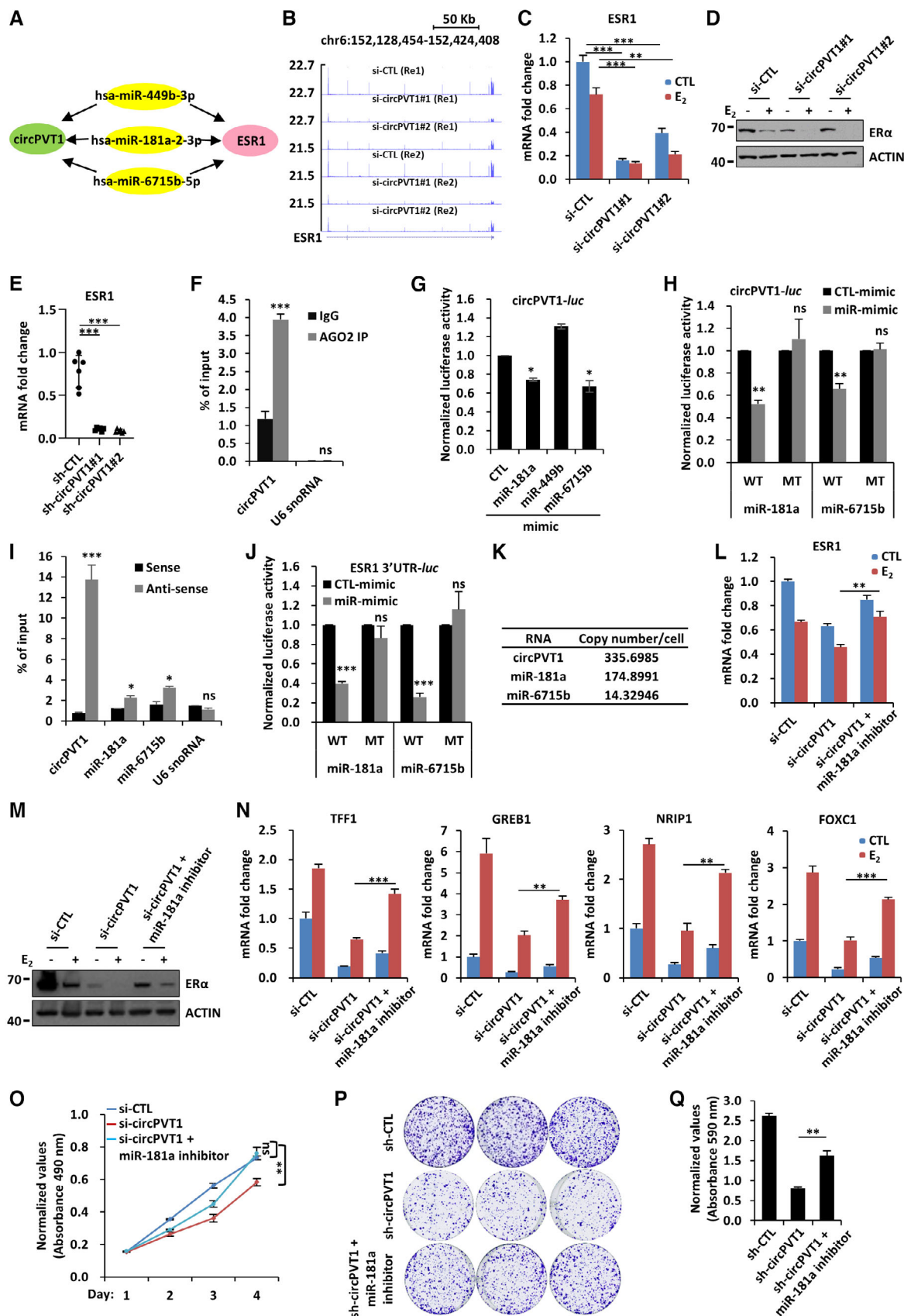


Figure 4.

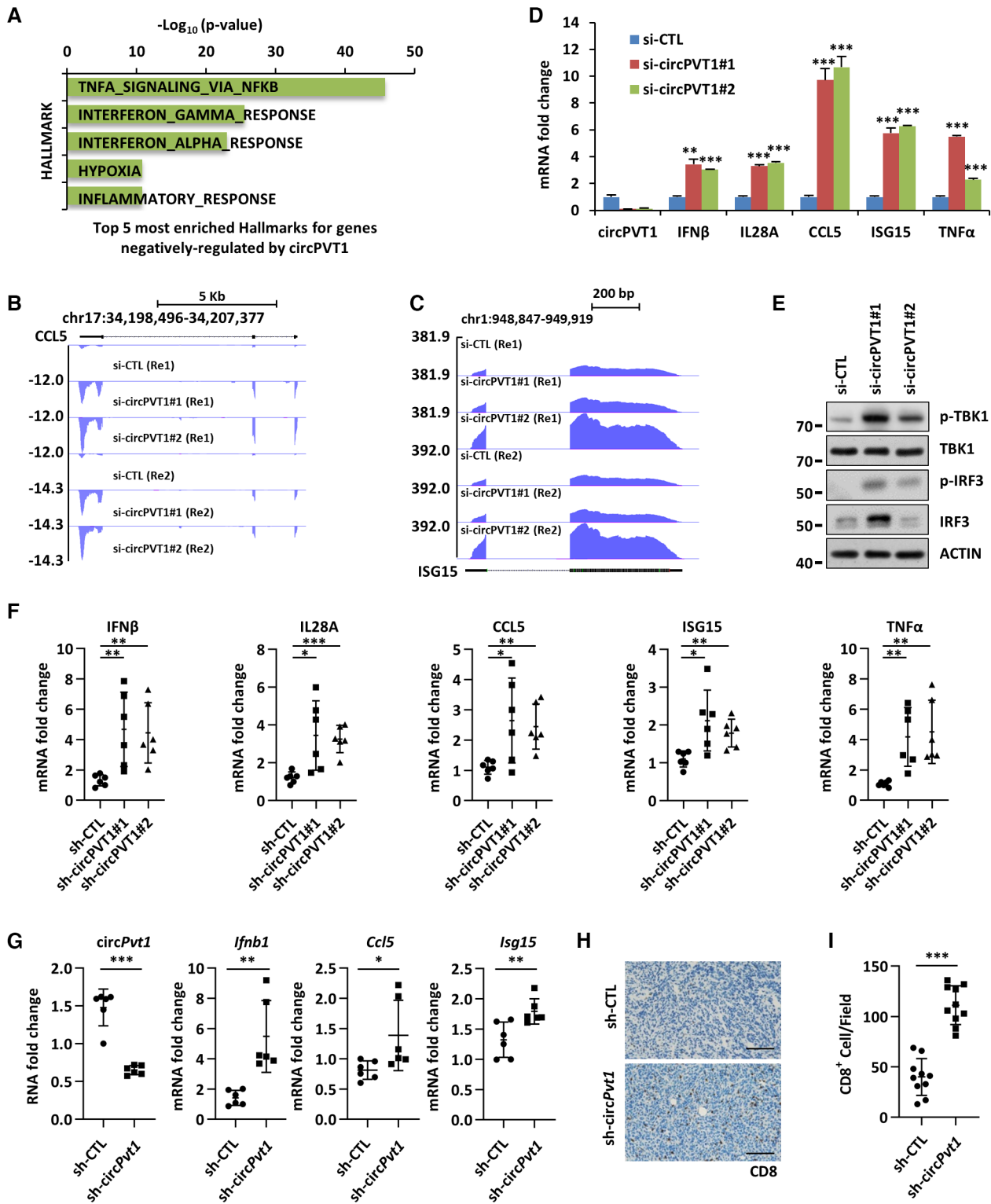


Figure 5.

CircPVT1 represses the expression of type I IFN and ISGs

Our RNA-seq analysis results revealed that a cohort of genes with implications in type I IFN signaling pathway were negatively

regulated by circPVT1 (Fig 5A-C), which were further confirmed by RT-qPCR analysis (Fig 5D). As expected, knockdown of circPVT1 led to the increased levels of phosphorylated-TBK and -IRF3 (Fig 5E). Similar results were also observed in T47D cells (Fig EV3A

Figure 5. CircPVT1 represses the expression of type I IFN and ISGs.

- A The five most enriched hallmark terms for genes negatively regulated by circPVT1 are shown.
- B, C UCSB genome browser views of RNA-seq as described in Fig 3A for *CCL5* (B) and *ISG15* (C) are shown.
- D, E MCF7 cells were transfected with control siRNA (si-CTL) or two individual siRNAs specific against circPVT1 (si-circPVT1#1 and si-circPVT1#2) were subjected to RT-qPCR analysis (D) to examine the expression of genes as indicated and immunoblotting analysis (E) using antibodies as indicated ($n = 3$ biological replicates, \pm s.e.m., $^{**}P < 0.01$, $^{***}P < 0.001$ by two-tailed Student's *t*-test).
- F Tumor samples as described in Fig 1K were subjected to RT-qPCR analysis to examine the expression of genes as indicated ($n = 6$ biological replicates, \pm s.e.m., $^{*}P < 0.05$, $^{**}P < 0.01$, $^{***}P < 0.001$ by two-tailed Student's *t*-test).
- G, H Tumor samples as described in Fig 1M were subjected to RNA extraction and RT-qPCR analysis (G) to examine the expression of genes as indicated and immunohistochemistry analysis (H) using anti-CD8 antibody. Dark brown staining indicates CD8-positive cell. Scale bar, 100 μ m ($n = 6$ biological replicates, \pm s.e.m., $^{*}P < 0.05$, $^{**}P < 0.01$, $^{***}P < 0.001$ by two-tailed Student's *t*-test).
- I The quantification of CD8-positive cells as described in (H) is shown ($n = 3$ biological replicates, mean \pm s.e.m., $^{***}P < 0.001$ by two-tailed Student's *t*-test).

and B). In consistent with its high expression in other subtypes of breast cancer cells, knockdown of circPVT1 in HCC1937 and 4T1 cells also led to the activation of type I IFN signaling (Fig EV3C–F). To support the functional importance of these type I IFN and ISGs in tumor development, the expression of representative ones was found to be significantly upregulated when circPVT1 was knocked down in MCF7 cell-derived xenografts (Figs 1K and 5F) and 4T1 cell-derived allografts (Figs 1M and 5G). CD8⁺ T cell infiltration was significantly increased when circPvt1 was knocked down (Figs 1M and 5H and I). Taken together, our data demonstrated that circPVT1 represses the expression of type I IFNs and ISGs in breast cancers.

CircPVT1 interrupts RIGI–MAVS interaction to repress the expression of type I IFN and ISGs

We next sought to investigate how circPVT1 engages in type I IFN signaling pathway. The activation of the type I IFN signaling pathway can be mediated through MAVS or STING proteins. We double knocked down circPVT1 and MAVS or STING in MCF7 cells, finding that knockdown of MAVS, but not STING, significantly attenuated the induced expression of *IFN β* , *IL28A*, *CCL5*, *ISG15*, and *TNF α* in circPVT1-knockdown cells (Figs 6A and EV4A and B). We then examined whether the repressive function of circPVT1 was dependent on cytoplasmic RNA sensors upstream of MAVS, including

MDA5 and RIGI. Double-knockdown experiment revealed that knockdown of RIGI, but not MDA5, significantly attenuated the phosphorylation of TBK1 and IRF3 as well as the expression of *IFN β* and ISGs in circPVT1-knockdown cells, suggesting that circPVT1 might target the RIGI–MAVS axis (Figs 6B and C, and EV4B–D). CircRNAs have been reported to function as protein scaffolds. The results of RIP analysis showed that circPVT1 was successfully pulled down by MAVS, but not by RIGI (Figs 6D and E, and EV4E and F). The interaction between circPVT1 and MAVS was further validated by Chromatin Isolation by RNA Purification (ChIRP) assay using biotin-labeled anti-sense probe specifically targeting circPVT1 (Fig 6F and G).

To characterize the interaction between circPVT1 and MAVS in detail, we transfected HEK293T cells with full length (FL), the amino (N)-terminal domain (NTD), or the carboxyl (C)-terminal domain (CTD) MAVS followed by RIP analysis. The results of RIP analysis revealed that circPVT1 interacted with the NTD in MAVS, but not the CTD (Fig 6H–K). Since the RNA sensor RIGI also interacts with the NTD of MAVS, we next determined whether circPVT1 will compete with RIGI for binding with MAVS. We transfected cells with RIGI and MAVS in the presence or absence of circPVT1 followed by immunoprecipitation (IP), and we found that the interaction between RIGI and MAVS was significantly blocked by circPVT1 (Fig 6L). It has been reported that MAVS will form prion-

Figure 6. CircPVT1 interrupts RIGI–MAVS interaction to repress the expression of type I IFN and ISGs.

- A MCF7 cells infected with control shRNA (sh-CTL) or shRNAs specifically targeting MAVS (sh-MAVS) or STING (sh-MAVS) were transfected with control siRNA (si-CTL) or siRNA specifically targeting circPVT1 (si-circPVT1) followed by RT-qPCR analysis to examine the expression of genes as indicated ($n = 3$ biological replicates, \pm s.e.m., ns: non-significant, $^{*}P < 0.05$, $^{**}P < 0.01$, $^{***}P < 0.001$ by two-tailed Student's *t*-test).
- B, C MCF7 cells infected with sh-CTL, sh-MAVS, sh-MDA5, or sh-RIGI were transfected with si-CTL or si-circPVT1 followed by immunoblotting analysis (B) using antibodies as indicated and RT-qPCR analysis (C) to examine the expression of genes as indicated ($n = 3$ biological replicates, \pm s.e.m., ns: non-significant, $^{*}P < 0.05$, $^{**}P < 0.01$, $^{***}P < 0.001$ by two-tailed Student's *t*-test).
- D, E RNA immunoprecipitation (RIP) was performed in MCF7 by using control IgG or anti-MAVS antibody followed by immunoblotting analysis (D) using antibodies as indicated and RT-qPCR analysis (E) to examine the binding of MAVS with circPVT1 and 7SK snRNA ($n = 3$ biological replicates, \pm s.e.m., $^{***}P < 0.001$ by two-tailed Student's *t*-test).
- F, G ChIRP analysis was performed in MCF7 cells with sense or anti-sense probe specifically targeting the junction region of circPVT1 followed by RT-qPCR analysis (F) to examine the RNA molecules being pulled down as indicated and immunoblotting analysis (G) to examine the interaction between MAVS and circPVT1 ($n = 3$ biological replicates, \pm s.e.m., ns: non-significant, $^{**}P < 0.01$ by two-tailed Student's *t*-test).
- H Schematic representation of MAVS protein is shown. CARD: caspase activation and recruitment domain; PRO: proline-rich domain; TM: transmembrane domain; NTD: amino-terminal domain; CTD: carboxyl-terminal domain.
- I–K HEK293T cells transfected with HA-tagged MAVS-FL, MAVS-NTD, or MAVS-CTD were subjected to RIP using anti-HA antibody followed by RT-qPCR analysis to examine the binding of circPVT1 (I) and 18 s rRNA (J) or immunoblotting analysis (K) using antibodies as indicated ($n = 3$ biological replicates, \pm s.e.m., $^{*}P < 0.05$, $^{**}P < 0.01$ by two-tailed Student's *t*-test). Asterisks indicate the predicted size of the corresponding proteins.
- L HEK293T cells transfected with HA-tagged MAVS and Flag-tagged RIGI in the presence or absence of circPVT1 were subjected to immunoprecipitation (IP) with anti-Flag M2 agarose followed by immunoblotting analysis using antibodies as indicated.
- M MCF7 cells transfected with si-CTL, si-circPVT1#1, or si-circPVT1#2 were subjected to SDD-AGE and SDS-PAGE analysis using antibodies as indicated.

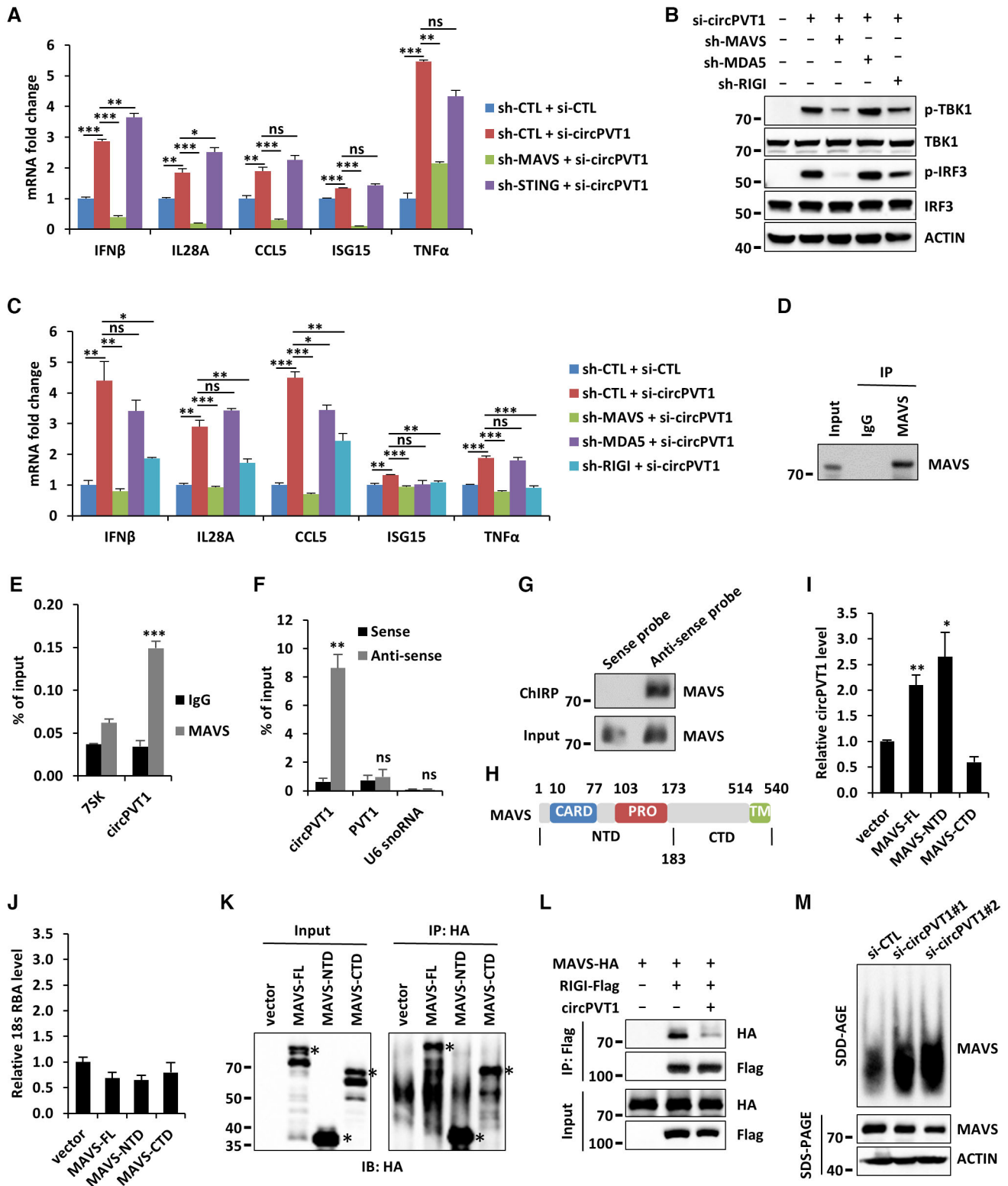


Figure 6.

like aggregates upon binding with RIGI (Hou *et al*, 2011). We thus tested whether the aggregation of MAVS will be influenced by circPVT1. The results of semi-denaturing detergent agarose gel electrophoresis (SDD-AGE) showed that the formation of aggregated

MAVS was dramatically enhanced in circPVT1-knockdown MCF7 cells (Fig 6M). Taken together, our data suggested that circPVT1 competes with RIGI to bind with MAVS, thus inhibiting the downstream signaling transduction and type I IFN and ISGs expression.

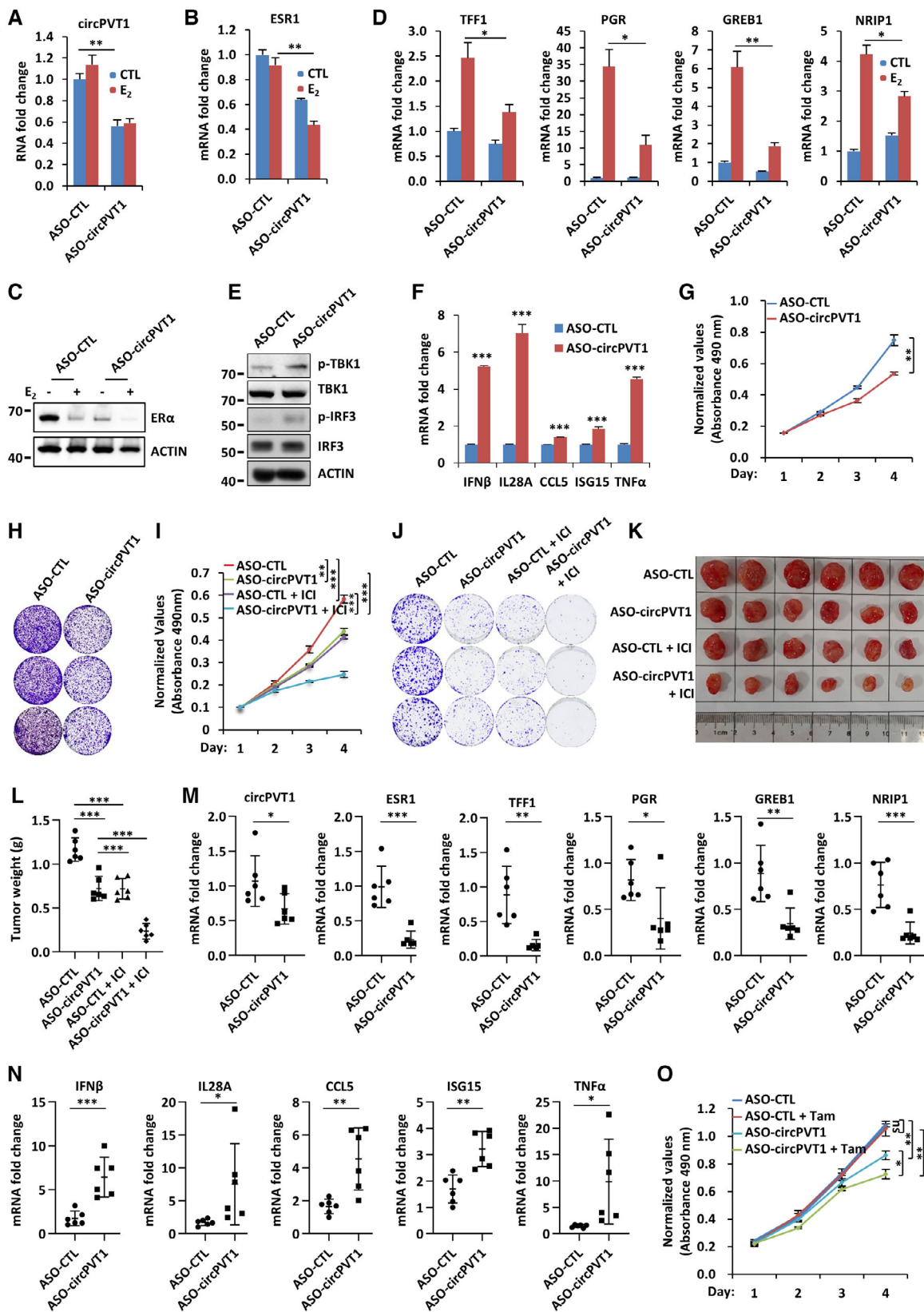


Figure 7.

Figure 7. Therapeutic anti-sense oligonucleotide (ASO)-targeting circPVT1 is effective in suppressing breast cancer cell growth and tumorigenesis.

- A–F MCF7 cells transfected with control ASO (ASO-CTL) or ASO specifically targeting circPVT1 (ASO-circPVT1) were subjected to RT-qPCR analysis (A, B, D, F) to examine the expression of genes as indicated and immunoblotting analysis (C, E) using antibodies as indicated ($n = 3$ biological replicates, \pm s.e.m., $*P < 0.05$, $**P < 0.01$, $***P < 0.001$ by two-tailed Student's *t*-test).
- G, H Cells as described in (A) were subjected to cell proliferation (G) and colony formation assay (H) ($n = 3$ biological replicates, \pm s.e.m., $**P < 0.01$, day 4 by two-tailed Student's *t*-test).
- I, J MCF7 cells were treated with ASO-CTL, ASO-circPVT1 (50 nM), or fulvestrant (ICI, 1 μ M) for duration as indicated followed by cell proliferation assay (I) and colony formation (J) ($n = 3$ biological replicates, \pm s.e.m., $**P < 0.01$, $***P < 0.001$, day 4 by two-tailed Student's *t*-test).
- K, L MCF7 cells were injected subcutaneously into female BALB/C nude mice, randomized, and then treated with estrogen in the presence of fulvestrant (ICI, 5 mg per dose, weekly) and/or ASO-circPVT1 (5 nm per dose, every 3 days). Tumors were then excised, photographed (K), and weighted (L) 4 weeks after subcutaneous injection ($n = 6$, \pm s.e.m., $***P < 0.001$ by two-tailed Student's *t*-test).
- M, N Tumor samples as described in (K) were subjected to RNA extraction and RT-qPCR analysis to examine the expression of genes as indicated ($n = 6$ biological replicates, \pm s.e.m., $*P < 0.05$, $**P < 0.01$, $***P < 0.001$ by two-tailed Student's *t*-test).
- O Tamoxifen-resistant MCF7 cells transfected with ASO-CTL or ASO-circPVT1 and treated with or without tamoxifen (Tam, 5 μ M) were subjected to cell proliferation assay ($n = 3$ biological replicates, \pm s.e.m., ns: non-significant, $*P < 0.05$, $**P < 0.01$, day 4 by two-tailed Student's *t*-test).

CircPVT1 serves as a potential therapeutic target for breast cancer

Anti-sense oligonucleotides (ASO) drugs were quickly developing during the past decades. ASO drugs, such as Vitravene and Nusinersen, have been approved by FDA for clinical use (Stein & Castanotto, 2017; Kulkarni *et al*, 2021; Alhamadani *et al*, 2022). The upregulation of circPVT1 in breast cancer cells and clinical sample and its significant role in ER α -positive breast cancer prompted us to examine whether circPVT1 can serve as a potential therapeutic target. ASO-circPVT1 significantly knocked down circPVT1 itself (Fig 7A) as well as its target, *ESR1*, at both mRNA and protein level (Fig 7B and C). As expected, estrogen/ER α -target genes were significantly decreased upon ASO-circPVT1 transfection (Fig 7D). Similarly, circPVT1-regulated phosphorylation of TBK1 and IRF3 (Fig 7E) and expression of type I IFN and ISGs (Fig 7F) were dramatically increased upon ASO-circPVT1 transfection. Consequently, ASO-circPVT1 could inhibit MCF7 cell growth (Figs 7G and H, and EV5A). Furthermore, combination treatment with ASO-circPVT1 and ICI exhibited synergistic effects on cell growth compared to treatment with either ASO-circPVT1 or ICI alone (Figs 7I and J, and EV5B).

To further test the therapeutic effects of ASO-circPVT1 *in vivo*, MCF7 cells were inoculated subcutaneously into female BALB/C nude mice followed by ASO treatment. ASO-circPVT1 treatment led to a significant decrease of tumor growth (Figs 7K and L, and EV5C). Combination treatment with ASO-circPVT1 and ICI exhibited synergistic effects on tumor growth (Figs 7K and L, and EV5C). The expression of *ESR1*, *TFF1*, *PGR*, *GREB1*, and *NR1P1* was found to be significantly inhibited upon ASO-circPVT1 treatment in tumors (Fig 7M). Meanwhile, the expression of *IFN β* , *IL28A*, *CCL5*, *ISG15*, and *TNF α* was upregulated (Fig 7N). Lastly, we found that ASO-circPVT1 could re-sensitize tamoxifen-resistant-MCF7 cells to tamoxifen treatment (Fig 7O). Taken together, our data suggested that ASO-targeting circPVT1 is as effective as fulvestrant to suppress ER α -positive breast cancer cell growth and tumorigenesis, and it can overcome endocrine therapy resistance.

Discussion

ER-positive breast cancer accounts for around two-thirds of all breast cancer subtypes. Although endocrine therapy can achieve

gratifying curative effects in patients with ER-positive breast cancer, there is still a persistent risk of resistance and recurrence. Here, we reported that a cytosolic localized circRNA, circPVT1, activates estrogen/ER α -target genes through sponging miR-181a-2-3p to stabilize *ESR1*, while it represses type I IFNs and ISGs through binding MAVS to disturb RIGI–MAVS complex formation. The dual functions of circPVT1 in both gene transcriptional activation and repression together contribute to ER α -positive breast cancer development. ASO-targeting circPVT1 is effective in suppressing ER α -positive breast tumor growth (Fig 8).

Tens of thousands of circRNAs have been widely detected, validated, and explored in different cell lines, tissues, organs, and species. In this study, we examined the effects of a cohort of highly expressed circRNAs on cell growth in ER α -positive breast cancer cells. Some of these circRNAs have already been reported in other studies. For instance, circCDYL is specifically upregulated in the early stages of hepatocellular carcinoma (HCC) (Wei *et al*, 2020). Circ-ZKSCAN1 acts as a tumor suppressor to regulate cell proliferation, migration, and invasion in bladder cancer cells (Bi *et al*, 2020). CircPVT1 was first reported to be associated with senescence by modulating let-7 activity (Panda *et al*, 2017). More recently, circPVT1 was found to be upregulated in gastric cancer due to genomic amplification. It promotes cell proliferation by acting as a sponge for members of the miR-125 family (Chen *et al*, 2017). Knockdown of circPVT1 could also inhibit cancer cell proliferation in other cancer types, such as acute lymphoblastic leukemia (Hu *et al*, 2018), ovarian cancer (Sun *et al*, 2020), and glioblastoma (Chi *et al*, 2020). Other studies have also shown that circPVT1 plays a critical role in cell migration in cancers, such as breast cancer (Bian, 2019; Wang *et al*, 2020a), esophageal cancer (Zhong *et al*, 2019), and medullary thyroid cancer (Zheng *et al*, 2021). In addition, some reports also indicated that circPVT1 is involved in the regulation of chemotherapeutic drug sensitivity and resistance in cancer cells (Ghafouri-Fard *et al*, 2021). For example, the depletion of circPVT1 would increase the sensitivity of gastric cancer cells to Paclitaxel treatment (Liu *et al*, 2019). However, it remains unknown whether and how circPVT1 functions in ER α -positive breast cancer and whether targeting circPVT1 can suppress ER α -positive breast tumorigenesis and overcome endocrine therapy resistance.

CircPVT1 was found to be stably localized in the cytoplasm. We focused on studying its potential role as a miRNA sponge and protein scaffold. Based on the ceRNA network constituting of circPVT1-

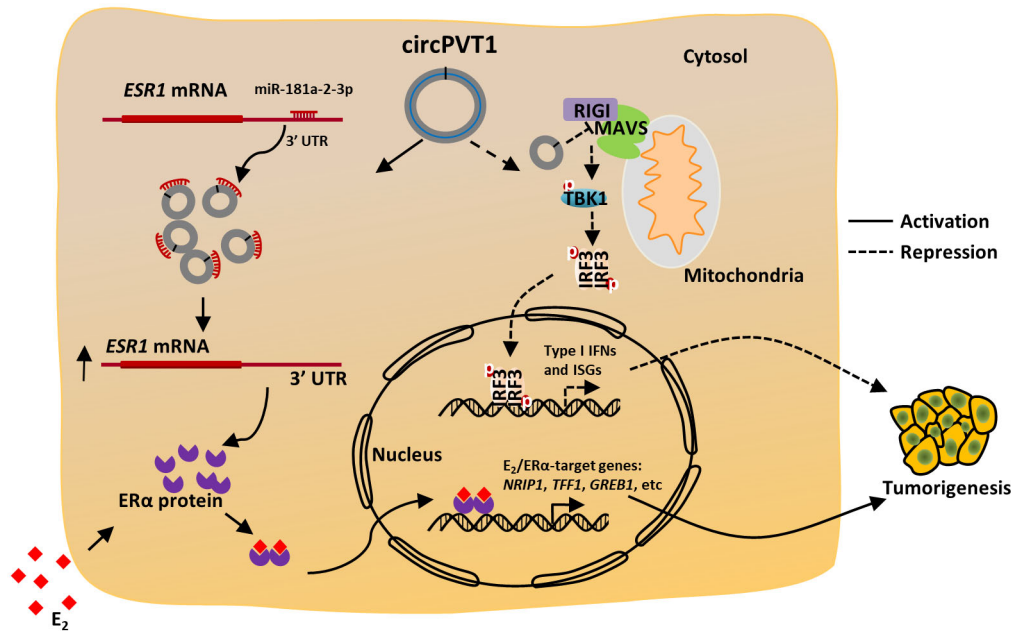


Figure 8. Working model of circPVT1 function in ER α -positive breast cancer.

A proposed model depicts that, in breast tumor cells, the highly expressed circPVT1 acts as a ceRNA to sponge miR-181a-2-3p to activate the expression of *ESR1* and downstream estrogen/ER α -target genes, while it interacts with MAVS to disturb the formation of RIGI–MAVS complex to inhibit the expression of type I IFN and ISGs. The dual function of circPVT1 in both gene transcriptional activation and repression together contributes to ER α -positive breast cancer development. ASO-targeting circPVT1 is effective in suppressing ER α -positive breast tumor growth.

miR-181a-2-3p-*ESR1* we constructed, we proved that circPVT1 promotes the expression of *ESR1* and ER α through miR-181a-2-3p. Thus, different from the mechanism of endocrine therapy for treating ER-positive breast cancer, targeting circPVT1 will directly inhibit the expression of ER α at the mRNA level, which has the potential to overcome endocrine therapy resistance for ER-positive breast cancer.

For circPVT1 negatively regulated genes, we found that TNF α signaling via NF κ B, interferon γ response, interferon α response, and inflammatory response were among the top five most enriched gene ontology terms. All these genes actually belong to the type I IFN signaling pathway. MAVS and STING are engaged in the RNA- and DNA-mediated type I IFN signaling pathway, respectively. Double-knockdown experiment indicated that circPVT1 regulates type I IFN signaling pathway through RIGI–MAVS axis. RIP and ChIRP assay results revealed that circPVT1 directly interacts with MAVS. The N terminus of MAVS is made up with a CARD and PRO domain, and the C terminus has a TM domain. Interestingly, circPVT1 interacts with the N terminus of MAVS, which is also utilized by the RNA sensor protein RIGI to interact with MAVS. This provides the molecular basis for circPVT1 to inhibit the RIGI–MAVS-mediated type I IFN signaling pathway, such that circPVT1 competes with RIGI to interact with MAVS and therefore inhibits MAVS aggregation, the critical event for the activation of downstream type I IFN signaling pathway. We surveyed the breast cancer datasets in TCGA to explore the correlation between type I IFN gene signature with estrogen/estrogen receptor gene signature. Gene set enrichment analysis (GSEA) results showed that type I IFN-related signaling pathways, such as “Allograft Rejection,” “Inflammatory

Response,” “TNF α Signaling Via NF κ B,” and “Interferon γ Response,” were negatively correlated with the expression of *ESR1*. As expected, “Estrogen Response Early” and “Estrogen Response Late” signaling pathways were highly correlated with *ESR1* expression. However, whether estrogen/ER α can inhibit type I IFN responses, or vice versa, remain unknown, which will certainly be an interesting topic for future investigation. Nevertheless, we demonstrated that circPVT1 promotes the expression of estrogen/ER α -target genes to promote cell growth, while it inhibits the type I IFN signaling pathway to inhibit anti-tumor immunity. These dual mechanisms together contribute to circPVT1 function in breast cancer development. We must emphasize that circPVT1 is also found to be highly expressed in ER-negative breast cancer cell lines and tumor tissues, and it appears that the repression of type I IFN signaling pathway is a common mechanism for circPVT1 to promote tumor growth.

Type I IFN signaling pathway facilitates anti-tumor immunity by activating of cytotoxic T cells and NK cells infiltration to inhibit cancer development in various cancer models (Lin & Karin, 2007; Hanahan & Weinberg, 2011; Banoth & Cassel, 2018; Greten & Grivennikov, 2019; Liu & Gack, 2020). Immune checkpoint blockade therapy is one of the most successful immunotherapies, showing remarkable effects in the treatment of many types of cancer (Postow et al, 2015). More and more breast cancer immunotherapy studies have been in the preclinical or clinical trial stage (Schmid et al, 2019; Mittendorf et al, 2020; Tolaney et al, 2020; Lee et al, 2022). Enhancing anti-tumor immune response is one of the effective ways to improve the efficacy of immune checkpoint blockade therapy. Based on our findings that

circPVT1 negatively regulates type I IFN signaling pathway and targeting circPVT1 improves anti-tumor immunity. The possibility of targeting circPVT1 in combination with immune checkpoint blockade therapy for breast cancer is worthy of future study. Nevertheless, ASO-targeting circPVT1 is effective in suppressing the expression of estrogen/ER α -target genes, and meanwhile enhancing the expression of type I IFN and ISGs, both of which contribute to the inhibitory effects of ASO on breast cancer cell growth and tumorigenesis. More importantly, ASO-targeting circPVT1 is able to overcome endocrine therapy resistance in ER α -positive breast cancer cells.

Taken together, our data demonstrated that circPVT1 can work through both ceRNA and protein scaffold mechanisms to promote ER α -positive breast cancer development and endocrine therapy resistance, providing a diagnosis biomarker and therapeutic target for ER α -positive breast cancer in the clinic.

Materials and Methods

Clinical specimens and cell lines

Breast tumor tissues and matched adjacent normal tissues were obtained from patients who were diagnosed with breast cancer and who had undergone surgery at the Second Affiliated Hospital of Shantou University Medical College. Tissue samples were freshly frozen in dry ice and stored at -80°C until RNA extraction. The study was approved by the Institutional Ethics Committee of the Second Affiliated Hospital of Shantou University Medical College (ID: 2022-7). All research was performed in compliance with government policies and the Helsinki Declaration. Experiments were undertaken with the understanding and written consent of each subject.

Human and mouse breast cancer cell lines and human embryonic kidney cell line HEK293T were cultured in Dulbecco's modified Eagle medium (DMEM) (Biological Industries) or Roswell Park Memorial Institute 1640 (RPMI 1640) (Biological Industries). All medium was supplied with 10% fetal bovine serum (FBS) (Biological Industries) and 1% penicillin/streptomycin (Biological Industries) for cell culture. When treating cells with estrogen (Sigma-Aldrich, E2758), phenol red-free medium supplemented with 5% charcoal-treated FBS was used.

Cloning procedures

ShRNA-targeting circPVT1 (both human and mouse), MAVS, STING, MDA5, or RIGI was cloned into lenti-viral pLKO.1 vector with AgeI and EcoRI restriction enzymes ((shRNA-targeting sequence: GCTGGGCTTGAGGCTGATCT (sh-circPVT1#1); CAGCTGGGCTTGAGGCTGAT (sh-circPVT1#2); ATGTGGATGTTGTAGAGATTC (sh-MAVS); CATGGTCATATTACATCGGAT (sh-STING); CCAACAAGAAGCAGTGTATA (sh-MDA5); AGCACTTGTGGACCTTTAAA (sh-RIGI)); AGCTCCCTCTAAAATGTCTGA (sh-circPvt1)).

Full-length circPVT1 was cloned in pCD2.1-ciR vector (Genesee Biotech) with KpnI and BamHI restriction enzymes for over-expression. This vector contains complementary Alu sequences besides the two restriction enzyme sites. Linear circPVT1 will be co-transcribed with the Alu sequences, which will generate circPVT1 through back splicing. pCD2.1-circPVT1 plasmid was transfected

into cells by using Lipo Plus DNA transfection reagent (Sagecreation).

Linear sequence of circPVT1 (circPVT1 (WT)) and its mutant form with the potential miR-181a-2-3p or miR-6715b-5p binding site mutated (circPVT1 (MT)) were cloned into psiCHECK2 vector with NotI and XhoI restriction enzymes, which were named as circPVT1 (WT)-*luc* and circPVT1 (MT)-*luc*, respectively. The primer used to mutate miR-181a-2-3p-binding site was TTATGTCAGATCTAGT-CACCTCTGGGAATAACGCTG, the primer used to mutate miR-6715b-5p-binding site was CCTCAAGATGGCTCACGGACACAGCTG-CATGGA. 3' untranslated region (3' UTR) of *ESR1* and the corresponding mutant form with the predicted miR-181a-2-3p or miR-6715b-5p binding site mutated were cloned into psiCHECK2 vector with NotI and XhoI restriction enzymes, which were named as 3' UTR (WT)-*luc* and 3' UTR (MT)-*luc*, respectively. The primer used to mutate miR-181a-2-3p-binding site was AGAACGGTGACTCC-CATTAGCTACTGTC. The primer used to mutate miR-6715b-5p-binding site was AGTTGTCCGTGCTTTGGATGCAAAA.

C-terminal HA-tagged full-length (FL) MAVS and truncations, NTD (1-183 aa) and CTD (174-540 aa), were cloned into pBoBics2.0 vector with BamHI and XhoI restriction enzymes. C-terminal Flag-tagged RIGI was kindly provided by Dr. Jiahui Han.

SiRNA, anti-sense oligonucleotides (ASO), miRNA inhibitor, miRNA mimic, and plasmid transfection, and lenti-virus packaging and infection

SiRNAs or anti-sense oligonucleotides (ASO) specifically targeting circPVT1 were purchased from RiboBio (siRNA-targeting sequence: GCUGGGCUUGAGGCCUGAU dTdT (si-circPVT1#1); UGGGCUUGAGGCCUGAUCU dTdT (si-circPVT1#2); ASO-targeting sequence: cholesterol modified-CTTGAGGCTGATCTTTGG (ASO-circPVT1)). The phosphorothioate backbone was used along the entire length of the ASO to provide nuclease resistance, while the 2'-O-methyl modification is used exclusively on the first and last 5 nucleotides, leaving the middle 10 nucleotides unmodified at the 2'-sugar position. This provides increased target RNA-binding affinity on the outer portions of the ASO, while still allowing RNase H cleavage at the central region of the ASO. MiR-181a-2-3p mimic and inhibitor were also purchased from RiboBio. SiRNA, ASO, miRNA inhibitor, and miRNA mimic transfections were performed using Lipofectamine 2000 (Invitrogen) according to the manufacturer's protocol. Plasmid transfections in HEK293T cells were performed using Polyethyleneimine (Polysciences, PEI) according to the manufacturer's protocol. Plasmid transfection in MCF7 cells was performed using Lipo Plus reagent according to the manufacturer's protocol. For lenti-virus packaging, HEK293T cells were seeded in culture plates coated with poly-D-lysine (0.1% (w/v), Sigma-Aldrich, P7280) and transfected with lenti-viral vectors together with packaging vectors, pMDL, VSVG, and REV, at a ratio of 10:5:3:2 using PEI for 48 h according to the manufacturer's protocol. Virus was collected, filtered, and added to MCF7 or 4T1 cells in the presence of 10 $\mu\text{g}/\text{ml}$ polybrene (Sigma-Aldrich, H9268), followed by centrifugation for 30 min at 1,500 g at 37°C . Medium was replaced 24 h later.

RNA isolation and RT-qPCR

Total RNA was isolated using TRIzol (Invitrogen) following the manufacturer's protocol. First-strand cDNA synthesis from total

RNA was carried out using GoScript™ Reverse Transcription Mix with random primers (Promega), followed by quantitative PCR (qPCR) using AriaMx Real-Time PCR machine (Agilent Technologies). All RT-qPCRs were repeated at least three times, and the relative abundance of each transcript was normalized to the expression level of ACTIN. Sequence information for all primers used to check both gene expression and circPVT1 expression was presented in Table EV1.

RNA sequencing (RNA-seq) and circRNA sequencing (circRNA-seq)

Total RNA was isolated using RNeasy Mini kit (Qiagen) following the manufacturer's protocol. DNase I in column digestion was included to ensure RNA quality. For circRNA-seq, total RNA after DNase I treatment was digested with RNase R (Epicenter) at 37°C for 3 h before RNA library preparation. RNA library preparation for both regular RNA-seq and circRNA-seq was performed by using NEBNext® Ultra™ Directional RNA Library Prep Kit for Illumina (E7420L).

For regular RNA-seq, paired-end sequencing was performed with Illumina HiSeq 4000 platform. Sequencing reads were aligned to the hg19 reference genome by using STAR. featureCounts was used to calculate the expression of RefSeq annotated genes with the options –primary (count primary alignments only), –B (only count read pairs that have both ends aligned), –C (do not count read pairs that have their two ends mapping to different chromosomes or mapping to same chromosomes but on different strands), –Q 20 (the minimum mapping quality score 20), and –s 0 (unstranded), and edgeR was used to determine the differentially expressed genes. For differentially expressed genes between sample groups, a cutoff of q value less than 0.05 and fold change larger than 1.5 was applied. Volcano plot and heat map were generated by R software. Hallmark analysis was performed using R package clusterProfiler.

For circRNA-seq analysis, sequencing reads were mapped to hg19 reference genome by using BWA MEM (–T 19), and circRNAs were predicted by using CIRI2.pl (Gao *et al*, 2017), find_circ (Memczak *et al*, 2013), and CIRCexplorer2 (Zhang *et al*, 2016). All three algorithms were used at default settings.

Competitive endogenous RNA (CeRNA) network analysis

To construct ceRNA network, miRNAs that could bind to circPVT1 were first predicted by using four independent algorithms, miRanda (default settings) (Betel *et al*, 2008), RNAhybrid (minimal free energy, –e – 23) (Rehmsmeier *et al*, 2004), TarPmiR (probability of target site, –p 0.8) (Ding *et al*, 2016), and RegRNA2 (Chang *et al*, 2013), based on miRBase. The miRNAs that were commonly predicted were chosen for downstream analysis. To construct the ceRNA network for circPVT1, only the mRNA targets that were shown to be positively regulated by circPVT1 were kept. The ceRNA network was constructed by Cytoscape (Shannon *et al*, 2003).

Cell proliferation assay

Cell viability was measured by using a CellTiter 96 AQueous one solution cell proliferation assay kit (Promega) following the manufacturer's protocol. Briefly, MCF7 and T47D cells were transfected with indicated siRNA or plasmid and maintained in culture medium for different time points followed by cell proliferation assay.

Colony formation assay

Cells were seeded at the same density (~2,000 cells/well) in 6-well plate and infected with lenti-viral shRNA, and medium was replaced 24 h later. Cells were then cultured in a humidified, 5% CO₂ atmosphere incubator at 37°C for 2–3 weeks until colonies developed. The cells were fixed in fixative solution (acetic acid: methanol = 1:3) for 15 min and stained with 0.1% crystal violet for 15 min. For quantification, the crystal violet dye was released into 10% acetic acid and data were recorded at wavelength 590 nm.

Mouse tumor models

Three groups (6 mice/group) of female BALB/C nude mice (age 4–6 weeks) were subcutaneously implanted with 1×10^7 of sh-CTL, sh-circPVT1#1, sh-circPVT1#2-infected MCF7 cells suspended in PBS. Each nude mouse was brushed with estrogen (E₂, 10^{–2} M) every 3 days for the duration of the experiments to sustain xenograft tumor growth. All mice were euthanized 20 days after subcutaneous injection. Tumors were then excised, photographed, and weighted. For xenograft assays to assess the effects of ASO or ICI treatment, four groups (6 mice/group) of female BALB/C nude mice (age 4–6 weeks) were subcutaneously implanted with 1×10^7 of MCF7 cells suspended in PBS. Each nude mouse was brushed with estrogen (E₂, 10^{–2} M) every 3 days for the duration of the experiments to sustain xenograft tumor growth. After 1 week, mice were randomized to treatment group based on tumor size and administrated with or without ICI (5 mg per dose, weekly) in the presence or absence of ASO-circPVT1 (5 nM per dose, every 3 days) for another 3 weeks. Tumors were measured, both long diameter (D) and short diameter (d), every 3 days with a caliper once palpable. Tumor volume was determined using the volume formula for an ellipsoid: $1/2 \times D \times d^2$. All mice were euthanized 4 weeks after subcutaneous injection. For 4T1 cell-derived allograft experiment, two groups (6 mice/group) female BALB/C mice (age 4–6 weeks) were subcutaneously implanted with 5×10^5 of sh-CTL or sh-circPvt1-infected 4T1 cells suspended in PBS. Tumors were measured as described above. Mice were sacrificed when tumors reached 1,500 mm³ or upon tumor ulceration/bleeding. Tumors were then excised, photographed, and weighted. Animals were housed in the Animal Facility at Xiamen University under pathogen-free conditions, following the protocol approved by the Xiamen Animal Care and Use Committee.

RNA fluorescence in situ hybridization (RNA-FISH)

MCF7 cells seeded on cover glass were transfected with siRNAs for 48 h before fixing with fixation buffer (4% formaldehyde, 10% acetic acid) for 10 min. Cells were then permeabilized in 70% of ethanol overnight and rehydrated in 2 × SSC buffer (300 mM NaCl and 30 mM sodium citrate [pH7.0]) with 50% formamide. Hybridization was carried out in the presence of 30 ng of probe (Sangon Biotech, biotin-GATCAGGCCTCAAGCCCAGCTG) at 37°C overnight. Biotin-labeled probes were incubated with Streptavidin-Cy3™ (Sigma-Aldrich, S6402) in 2 × SSC buffer with 8% formamide, 2 mM vanadyl-ribonucleoside complex, and 0.2% RNase-free BSA at 37°C for 1 h in dark. Nuclei were counterstained with DAPI (0.1 µg/ml) and then washed twice with 2 × SSC with 8% formamide at room temperature (RT) for 15 min. Three images of each

cover glass were taken with Carl Zeiss laser confocal microscope, and representative images were shown.

Cellular fractionation

Cellular fractionation was performed as described previously (Gao *et al.*, 2015). Briefly, cells were washed with ice-cold PBS, collected, spun down, and re-suspended in ice-cold buffer I (10 mM Hepes (pH 8.0), 1.5 mM MgCl₂, 10 mM KCl, and 1 mM DTT) supplemented with protease inhibitor cocktail (Roche) and RNase inhibitor (Promega), followed by incubation for 15 min on ice to allow cells to swell. Igepal-CA630 was then added at a final concentration of 1% (use 10% stock solution) followed by vortexing for 10 s. Nuclei were collected by centrifuging 2 ~ 3 min at maximum speed. The resultant supernatant was cytosolic fraction. Nuclei were then lysed in ice-cold buffer II (20 mM Hepes (pH 8.0), 1.5 mM MgCl₂, 25% glycerol, 420 mM NaCl, 0.2 mM EDTA, and 1 mM DTT) supplemented with protease inhibitor cocktail and RNase inhibitor followed by vigorous rotation at 4°C for 30 min and centrifugation 15 min at maximum speed. The resultant supernatant was nuclear fraction. Both cytosolic and nuclear RNAs were extracted by Phenol-Chloroform-Isoamyl Alcohol mixture (Sigma-Aldrich, 77618) followed by RT-qPCR analysis.

RNase R digestion

Total RNAs were isolated by TRIzol which were treated with RNase R (10 units/μg RNA) in RNase R buffer supplemented with murine Ribonuclease Inhibitor (New England Biolabs) at 37°C for 1 h, 3 h, or 6 h, and followed by RT-qPCR analysis.

RNA immunoprecipitation (RIP)

RIP was performed as described previously (Jia *et al.*, 2016). Briefly, cells were lysed in polysome lysis buffer (100 mM KCl, 5 mM MgCl₂, 10 mM HEPES (pH 7.0), 0.5% NP-40, 1 mM DTT, and 2 mM vanadyl-ribonucleoside complexes solution [Sigma-Aldrich, 94742]) supplemented with protease inhibitor cocktail and RNase inhibitor, which were then subjected to IP with indicated antibody, and followed by washing with polysome lysis buffer four times and polysome lysis buffer plus 1 M urea four times. RNAs was released by adding 150 μL of polysome lysis buffer with 0.1% SDS and 45 μg proteinase K (Ambion, AM2548) and incubated at 50°C for 30 min. RNA extracted with phenol-chloroform-isoamyl alcohol mixture was recovered by adding 2 μL GlycoBlue (15 mg/ml, Ambion), 36 μL 3 M sodium acetate, and 750 μL ethanol followed by incubation at -20°C for overnight. Precipitated RNAs were washed with 70% ethanol, air dried, and re-suspended in RNase-free water followed by DNase I (Promega, M6101) treatment to remove genomic DNA. The resultant RNAs were subjected to RT-qPCR analysis.

Anti-sense or sense probe pull-down and chromatin isolation by RNA purification (ChIRP) assay

Oligonucleotide pull-down was carried out as described previously (Panda *et al.*, 2017). MCF7 cells were lysed in polysome extraction buffer (PEB, 20 mM Tris-HCl (pH 7.5), 100 mM KCl, 5 mM MgCl₂, and 0.5% NP-40) supplemented with protease inhibitor cocktail and RNase inhibitor for 10 min on ice, and the supernatant was collected

by centrifugation for 10 min at 15,000 g at 4°C, which were then incubated with 100 pM of biotin-labeled sense oligonucleotide (biotin-CAGCTGGGCTTGAGGCCTGATC) or an anti-sense oligonucleotide complementary to the junction sequence of circPVT1 (biotin-GATCAGGCCTCAAGCCCAGCTG) in 1 × TENT buffer (10 mM Tris-HCl [pH 8.0], 1 mM EDTA [pH 8.0], 250 mM NaCl, and 0.5% Triton X-100 [v/v]) supplemented with protease inhibitor cocktail and RNase inhibitor at 25°C for 1 h with rotation. Streptavidin-coupled Dynabeads (Invitrogen, M280) were washed with 1 × TENT buffer and incubated with lysates at 25°C for 30 min with rotation. After washing the beads three times with ice-cold 1 × TENT buffer, RNA was isolated using TRIzol, and circPVT1, PVT1, and microRNAs in the pull-down were detected by RT-qPCR analysis. For ChIP assay, RNA-binding proteins were detected by immunoblotting.

Immunoblotting and immunoprecipitation

Immunoblotting analysis was performed following the protocol described previously (Gao *et al.*, 2018). Antibodies used are listed as follows: Anti-ERα (Santa Cruz Biotechnology, sc-543), anti-ACTIN (Proteintech, 66009-1-Ig), anti-TBK1 (Santa Cruz Biotechnology, sc-52957), anti-IRF3 (Santa Cruz Biotechnology, sc-33641), anti-p-TBK1 (Cell Signaling Technology, 5483S), anti-p-IRF3 (Cell Signaling Technology, 4947S), anti-MAVS (Proteintech, 14341-1-AP), anti-STING (Cell Signaling Technology, 13647S), anti-MDA5 (Proteintech, 21775-1-AP), anti-RIGI (Cell Signaling Technology, D14G6), anti-HA (Roche, 3F10), anti-HA (Abcam, ab9110), anti-Flag (Sigma-Aldrich, F1804), and anti-Flag M2 Affinity Gel (Millipore, A2220, for immunoprecipitation).

Copy number analysis

Copy number analysis was performed following the protocol reported previously with minor modifications (Castellanos-Rubio *et al.*, 2016). Briefly, MCF7 cells cultured in stripping medium for 3 days were treated with estrogen (E₂, 10⁻⁷ M) for 6 h, and 1.5 × 10⁶ cells were then used for copy number analysis. Absolute quantification was performed using 2-fold serial dilutions of the reference standard, and Ct value from qPCR analysis versus the dilution factor was plotted, fitting the data to a straight line. The standard curve was used for extrapolating the number of molecules of interest.

Semidenaturing detergent agarose gel electrophoresis

Semidenaturing detergent agarose gel electrophoresis (SDD-AGE) was performed according to a published protocol (Hou *et al.*, 2011). Briefly, crude mitochondria were extracted and resuspended in sample buffer (0.5 × TBE, 10% glycerol, 2% SDS, and 0.0025% bromophenol blue) and loaded onto 1.5% agarose gel. After electrophoresis in the running buffer (1 × TBE and 0.1% SDS) for 35 min with a constant voltage of 100 V at 4°C, the proteins were transferred to immobilon membrane for immunoblotting.

Immunohistochemistry

Immunohistochemistry assay was performed following the protocol described previously (Shen *et al.*, 2021).

Statistics analysis

The comparison of two groups or data points was performed by the two-tailed *t*-test. Multiple comparisons were analyzed by two-way analysis of variance (ANOVA). $P \leq 0.05$ was considered statistically significant. Results from xenograft experiments and clinical breast samples were analyzed by GraphPad Prism 9.

Data availability

RNA-seq data were deposited in the Gene Expression Omnibus database under accession GSE220776 (<http://www.ncbi.nlm.nih.gov/geo/query/acc.cgi?acc=GSE220776>).

Expanded View for this article is available [online](#).

Acknowledgments

This work was supported by the National Natural Science Foundation of China (82125028, U22A20320, 31871319, 91953114, 81761128015, and 81861130370), the National Key Research and Development Program of China (2020YFA0112300 and 2020YFA0803600), the Natural Science Foundation of Fujian Province of China (2020J02004), and the Fundamental Research Funds for the Central University (20720190145 and 20720220003) to W. Liu. This work was also supported by the China Postdoctoral Science Foundation (2020M682097) to JY.

Author contributions

Jia Yi: Conceptualization; data curation; formal analysis; supervision; funding acquisition; validation; investigation; visualization; methodology; writing – original draft; writing – review and editing. **Lei Wang:** Conceptualization; data curation; formal analysis; supervision; validation; investigation; visualization; methodology; writing – original draft; writing – review and editing. **Guo-sheng Hu:** Data curation; software; formal analysis; investigation. **Yue-ying Zhang:** Validation; investigation; methodology; writing – review and editing. **Jiao Du:** Validation; investigation; writing – review and editing. **Jian-cheng Ding:** Software; validation. **Xiang Ji:** Validation. **Hai-feng Shen:** Validation; methodology; writing – review and editing. **Hai-hua Huang:** Resources. **Feng Ye:** Conceptualization; resources; supervision; validation; methodology; writing – original draft; writing – review and editing. **Wen Liu:** Conceptualization; resources; data curation; supervision; funding acquisition; investigation; visualization; writing – original draft; project administration; writing – review and editing.

Disclosure and competing interests statement

The authors declare that they have no conflict of interest.

References

- Ablasser A, Hur S (2020) Regulation of cGAS- and RLR-mediated immunity to nucleic acids. *Nat Immunol* 21: 17–29
- Ahmadani F, Zhang K, Parikh R, Wu HY, Rasmussen TP, Bahal R, Zhong XB, Manautou JE (2022) Adverse drug reactions and toxicity of the Food and Drug Administration-approved antisense oligonucleotide drugs. *Drug Metab Dispos* 50: 879–887
- Anurag M, Ellis MJ, Haricharan S (2018) DNA damage repair defects as a new class of endocrine treatment resistance driver. *Oncotarget* 9: 36252–36253
- Ashwal-Fluss R, Meyer M, Pamudurti NR, Ivanov A, Bartok O, Hanan M, Evantal N, Memczak S, Rajewsky N, Kadener S (2014) circRNA biogenesis competes with pre-mRNA splicing. *Mol Cell* 56: 55–66
- Banoth B, Cassel SL (2018) Mitochondria in innate immune signaling. *Transl Res* 202: 52–68
- Betel D, Wilson M, Gabow A, Marks DS, Sander C (2008) The microRNA.org resource: targets and expression. *Nucleic Acids Res* 36: D149–D153
- Bi JM, Liu HW, Dong W, Xie WB, He QQ, Cai ZJ, Huang J, Lin TX (2020) Circular RNA circ-ZKSCAN1 inhibits bladder cancer progression through miR-1178-3p/p21 axis and acts as a prognostic factor of recurrence (vol 18, 133, 2019). *Mol Cancer* 19: 148
- Bian Q (2019) Circular RNA PVT1 promotes the invasion and epithelial-mesenchymal transition of breast cancer cells through serving as a competing endogenous RNA for miR-204-5p. *Oncotargets Ther* 12: 11817–11826
- Blackburn SA, Parks RM, Cheung KL (2018) Fulvestrant for the treatment of advanced breast cancer. *Expert Rev Anticancer Ther* 18: 619–628
- Castellanos-Rubio A, Fernandez-Jimenez N, Kratchmarov R, Luo X, Bhagat G, Green PH, Schneider R, Kiledjian M, Bilbao JR, Ghosh S (2016) A long noncoding RNA associated with susceptibility to celiac disease. *Science* 352: 91–95
- Chang TH, Huang HY, Hsu JB, Weng SL, Horng JT, Huang HD (2013) An enhanced computational platform for investigating the roles of regulatory RNA and for identifying functional RNA motifs. *BMC Bioinformatics* 14: S4
- Chen LL (2016) The biogenesis and emerging roles of circular RNAs. *Nat Rev Mol Cell Biol* 17: 205–211
- Chen L-L (2020) The expanding regulatory mechanisms and cellular functions of circular RNAs. *Nat Rev Mol Cell Biol* 21: 475–490
- Chen YG, Hur S (2022) Cellular origins of dsRNA, their recognition and consequences. *Nat Rev Mol Cell Biol* 23: 286–301
- Chen Q, Sun L, Chen ZJ (2016) Regulation and function of the cGAS-STING pathway of cytosolic DNA sensing. *Nat Immunol* 17: 1142–1149
- Chen J, Li Y, Zheng QP, Bao CY, He J, Chen B, Lyu DB, Zheng BQ, Xu Y, Long ZW *et al* (2017) Circular RNA profile identifies circPVT1 as a proliferative factor and prognostic marker in gastric cancer. *Cancer Lett* 388: 208–219
- Chi G, Yang F, Xu D, Liu W (2020) Silencing hsa_circ_PVT1 (circPVT1) suppresses the growth and metastasis of glioblastoma multiforme cells by up-regulation of miR-199a-5p. *Artif Cells Nanomed Biotechnol* 48: 188–196
- Clarke R, Leonessa F, Welch JN, Skaar TC (2001) Cellular and molecular pharmacology of antiestrogen action and resistance. *Pharmacol Rev* 53: 25–71
- Ding J, Li X, Hu H (2016) TarPmiR: a new approach for microRNA target site prediction. *Bioinformatics* 32: 2768–2775
- Gao WW, Xiao RQ, Peng BL, Xu HT, Shen HF, Huang MF, Shi TT, Yi J, Zhang WJ, Wu XN *et al* (2015) Arginine methylation of HSP70 regulates retinoid acid-mediated RARBeta2 gene activation. *Proc Natl Acad Sci U S A* 112: E3327–E3336
- Gao Y, Zhang J, Zhao F (2017) Circular RNA identification based on multiple seed matching. *Brief Bioinform* 19: 803–810
- Gao WW, Xiao RQ, Zhang WJ, Hu YR, Peng BL, Li WJ, He YH, Shen HF, Ding JC, Huang QX *et al* (2018) JMJD6 licenses ERalpha-dependent enhancer and coding gene activation by modulating the recruitment of the CARM1/MED12 Co-activator complex. *Mol Cell* 70: e348
- Ge JS, Wang J, Xiong F, Jiang XJ, Zhu KJ, Wang YA, Mo YZ, Gong ZJ, Zhang SS, He Y *et al* (2021) Epstein-Barr virus-encoded circular RNA CircBART2.2 promotes immune escape of nasopharyngeal carcinoma by regulating PD-L1. *Cancer Res* 81: 5074–5088

- Ghafari-Fard S, Khoshbakht T, Taheri M, Jamali E (2021) A concise review on the role of CircPVT1 in tumorigenesis, drug sensitivity, and cancer prognosis. *Front Oncol* 11: 762960
- Green KA, Carroll JS (2007) Oestrogen-receptor-mediated transcription and the influence of co-factors and chromatin state. *Nat Rev Cancer* 7: 713–722
- Greten FR, Grivnenikov SI (2019) Inflammation and cancer: triggers, mechanisms, and consequences. *Immunity* 51: 27–41
- Hanahan D, Weinberg RA (2011) Hallmarks of cancer: the next generation. *Cell* 144: 646–674
- Hansen TB, Jensen TI, Clausen BH, Bramsen JB, Finsen B, Damgaard CK, Kjems J (2013) Natural RNA circles function as efficient microRNA sponges. *Nature* 495: 384–388
- Hou F, Sun L, Zheng H, Skaug B, Jiang QX, Chen ZJ (2011) MAVS forms functional prion-like aggregates to activate and propagate antiviral innate immune response. *Cell* 146: 448–461
- Howell A, Robertson JF, Abram P, Lichinitser MR, Elledge R, Bajetta E, Watanabe T, Morris C, Webster A, Dimery I et al (2004) Comparison of fulvestrant versus tamoxifen for the treatment of advanced breast cancer in postmenopausal women previously untreated with endocrine therapy: a multinational, double-blind, randomized trial. *J Clin Oncol* 22: 1605–1613
- Hu JJ, Han Q, Gu Y, Ma JL, McGrath M, Qiao FC, Chen BA, Song CH, Ge Z (2018) Circular RNA PVT1 expression and its roles in acute lymphoblastic leukemia. *Epigenomics* 10: 723–732
- Ishikawa H, Barber GN (2008) STING is an endoplasmic reticulum adaptor that facilitates innate immune signalling (vol 455, pg 674, 2008). *Nature* 456: 274
- Ishikawa H, Ma Z, Barber GN (2009) STING regulates intracellular DNA-mediated, type I interferon-dependent innate immunity. *Nature* 461: 788–792
- Jia Y, Hai-Feng S, Jin-Song Q, Ming-Feng H, Wen-Juan Z, Jian-Cheng D, Xiao-Yan Z, Yu Z, Xiang-Dong F, Wen L (2016) JMJD6 and U2AF65 co-regulate alternative splicing in both JMJD6 enzymatic activity dependent and independent manner. *Nucleic Acids Res* 45: 3503–3518
- Kristensen LS, Andersen MS, Stagsted LVW, Ebbesen KK, Hansen TB, Kjems J (2019) The biogenesis, biology and characterization of circular RNAs. *Nat Rev Genet* 20: 675–691
- Kristensen LS, Jakobsen T, Hager H, Kjems J (2022) The emerging roles of circRNAs in cancer and oncology. *Nat Rev Clin Oncol* 19: 188–206
- Kulkarni JA, Witzigmann D, Thomson SB, Chen S, Leavitt BR, Cullis PR, van der Meel R (2021) The current landscape of nucleic acid therapeutics. *Nat Nanotechnol* 16: 630–643
- Lee JV, Housley F, Yau C, Nakagawa R, Winkler J, Anttila JM, Munne PM, Savelius M, Houlahan KE, van de Mark D et al (2022) Combinatorial immunotherapies overcome MYC-driven immune evasion in triple negative breast cancer. *Nat Commun* 13: 3671
- Li J, Sun D, Pu W, Wang J, Peng Y (2020) Circular RNAs in cancer: biogenesis, function, and clinical significance. *Trends Cancer* 6: 319–336
- Lin WW, Karin M (2007) A cytokine-mediated link between innate immunity, inflammation, and cancer. *J Clin Invest* 117: 1175–1183
- Liu G, Gack MU (2020) Distinct and orchestrated functions of RNA sensors in innate immunity. *Immunity* 53: 26–42
- Liu Y-y, Zhang L-y, Du W-z (2019) Circular RNA circ-PVT1 contributes to paclitaxel resistance of gastric cancer cells through the regulation of ZEB1 expression by sponging miR-124-3p. *Biosci Rep* 39: BSR20193045
- Memczak S, Jens M, Elefsinioti A, Torti F, Krueger J, Rybak A, Maier L, Mackowiak SD, Gregersen LH, Munschauer M et al (2013) Circular RNAs are a large class of animal RNAs with regulatory potency. *Nature* 495: 333–338
- Mesa-Eguigaray I, Wild SH, Rosenberg PS, Bird SM, Brewster DH, Hall PS, Cameron DA, Morrison D, Figueroa JD (2020) Distinct temporal trends in breast cancer incidence from 1997 to 2016 by molecular subtypes: a population-based study of Scottish cancer registry data. *Br J Cancer* 123: 852–859
- Mittendorf EA, Zhang H, Barrios CH, Saji S, Jung KH, Hegg R, Koehler A, Sohn J, Iwata H, Telli ML et al (2020) Neoadjuvant atezolizumab in combination with sequential nab-paclitaxel and anthracycline-based chemotherapy versus placebo and chemotherapy in patients with early-stage triple-negative breast cancer (IMpassion031): a randomised, double-blind, phase 3 trial. *Lancet* 396: 1090–1100
- Motwani M, Pesiridis S, Fitzgerald KA (2019) DNA sensing by the cGAS-STING pathway in health and disease. *Nat Rev Genet* 20: 657–674
- Osborne CK (1998) Drug therapy – tamoxifen in the treatment of breast cancer. *N Engl J Med* 339: 1609–1618
- Palcau AC, Canu V, Donzelli S, Strano S, Pulito C, Blandino GJM (2022) CircPVT1: a pivotal circular node intersecting Long Non-Coding-PVT1 and c-MYC oncogenic signals. *Mol Cancer* 21: 1–15
- Pan HC, Gray R, Braybrooke J, Davies C, Taylor C, McGale P, Peto R, Pritchard KI, Bergh J, Dowsett M et al (2017) 20-year risks of breast-cancer recurrence after stopping endocrine therapy at 5 years. *N Engl J Med* 377: 1836–1846
- Panda AC, Grammatikakis I, Kim KM, De S, Martindale JL, Munk R, Yang X, Abdelmohsen K, Gorospe M (2017) Identification of senescence-associated circular RNAs (SAC-RNAs) reveals senescence suppressor CircPVT1. *Nucleic Acids Res* 45: 4021–4035
- Postow MA, Callahan MK, Wolchok JD (2015) Immune checkpoint blockade in cancer therapy. *J Clin Oncol* 33: 1974–1982
- Rehmsmeier M, Steffen P, Hochsmann M, Giegerich R (2004) Fast and effective prediction of microRNA/target duplexes. *RNA* 10: 1507–1517
- Rossinnes CS, Stark R, Teschendorff AE, Holmes KA, Ali HR, Dunning MJ, Brown GD, Gojis O, Ellis IO, Green AR et al (2011) Differential oestrogen receptor binding is associated with clinical outcome in breast cancer. *Nature* 481: 389–393
- Roulois D, Yau HL, Singhanian R, Wang YD, Danesh A, Shen SY, Han H, Liang GN, Jones PA, Pugh TJ et al (2015) DNA-Demethylating agents target colorectal cancer cells by inducing viral mimicry by endogenous transcripts. *Cell* 162: 961–973
- Schmid P, Chui SY, Emens LA (2019) Atezolizumab and nab-paclitaxel in advanced triple-negative breast cancer REPLY. *N Engl J Med* 380: 987–988
- Schneider WM, Chevillotte MD, Rice CM (2014) Interferon-stimulated genes: a complex web of host defenses. *Annu Rev Immunol* 32: 513–545
- Seth RB, Sun LJ, Ea CK, Chen ZJJ (2005) Identification and characterization of MAVS, a mitochondrial antiviral signaling protein that activates NF- κ B and IRF3. *Cell* 122: 669–682
- Shannon P, Markiel A, Ozier O, Baliga NS, Wang JT, Ramage D, Amin N, Schwikowski B, Ideker T (2003) Cytoscape: a software environment for integrated models of biomolecular interaction networks. *Genome Res* 13: 2498–2504
- Shen HF, Zhang WJ, Huang Y, He YH, Hu GS, Wang L, Peng BL, Yi J, Li TT, Rong R et al (2021) The dual function of KDM5C in both gene transcriptional activation and repression promotes breast cancer cell growth and tumorigenesis. *Adv Sci (Weinh)* 8: 2004635
- Sheng WQ, LaFleur MW, Nguyen TH, Chen SJ, Chakravarthy A, Conway JR, Li Y, Chen H, Yang H, Hsu PH et al (2018) LSD1 ablation stimulates anti-tumor immunity and enables checkpoint blockade. *Cell* 174: 549–563

- Shu C, Selmanoff MJN (1991) Effects of tumor-induced hyperprolactinemia on LH secretion following stimulation of the medial preoptic area, pituitary responsiveness and the estrogen-induced LH surge. *Neuroendocrinology* 54: 227–235
- Stein CA, Castanotto D (2017) FDA-approved oligonucleotide therapies in 2017. *Mol Ther* 25: 1069–1075
- Sun QM, Sun LJ, Liu HH, Chen X, Seth RB, Forman J, Chen ZJJ (2006) The specific and essential role of MAVS in antiviral innate immune responses. *Immunity* 24: 633–642
- Sun XF, Luo L, Gao YQ (2020) Circular RNA PVT1 enhances cell proliferation but inhibits apoptosis through sponging microRNA-149 in epithelial ovarian cancer. *J Obstet Gynaecol Res* 46: 625–635
- Tolaney SM, Barroso-Sousa R, Keenan T, Li TY, Trippa L, Vaz-Luis I, Wulf G, Spring L, Sinclair NF, Andrews C et al (2020) Effect of Eribulin with or without Pembrolizumab on progression-free survival for patients with hormone receptor-positive, ERBB2-negative metastatic breast cancer: a randomized clinical trial. *JAMA Oncol* 6: 1598–1605
- Waks AG, Winer EP (2019) Breast cancer treatment a review. *JAMA* 321: 288–300
- Wang J, Huang K, Shi L, Zhang Q, Zhang S (2020a) CircPVT1 promoted the progression of breast cancer by regulating MiR-29a-3p-mediated AGR2-HIF-1alpha pathway. *Cancer Manag Res* 12: 11477–11490
- Wang J, Huang K, Shi L, Zhang QY, Zhang SC (2020b) CircPVT1 promoted the progression of breast cancer by regulating MiR-29a-3p-mediated AGR2-HIF-1 alpha pathway. *Cancer Manag Res* 12: 11477–11490
- Wang L, Yi J, Lu LY, Zhang YY, Wang L, Hu GS, Liu YC, Ding JC, Shen HF, Zhao FQ et al (2021) Estrogen-induced circRNA, circPGR, functions as a ceRNA to promote estrogen receptor-positive breast cancer cell growth by regulating cell cycle-related genes. *Theranostics* 11: 1732–1752
- Wei YP, Chen X, Liang C, Ling Y, Yang XW, Ye XF, Zhang HL, Yang PH, Cui XL, Ren YB et al (2020) A noncoding regulatory RNAs network driven by Circ-CDYL acts specifically in the early stages hepatocellular carcinoma. *Hepatology* 71: 130–147
- West AP, Shadel GS, Ghosh S (2011) Mitochondria in innate immune responses. *Nat Rev Immunol* 11: 389–402
- Xia P, Wang S, Ye B, Du Y, Li C, Xiong Z, Qu Y, Fan Z (2018) A circular RNA protects dormant hematopoietic stem cells from DNA sensor cGAS-mediated exhaustion. *Immunity* 48: 688–701
- Yang Y, Fan X, Mao M, Song X, Wu P, Zhang Y, Jin Y, Yang Y, Chen LL, Wang Y et al (2017) Extensive translation of circular RNAs driven by N(6)-methyladenosine. *Cell Res* 27: 626–641
- Yum S, Li MH, Frankel AE, Chen ZJJ (2019) Roles of the cGAS-STING pathway in cancer Immunosurveillance and immunotherapy. *Annu Rev Cancer Biol* 3: 323–344
- Zhang XO, Dong R, Zhang Y, Zhang JL, Luo Z, Zhang J, Chen LL, Yang L (2016) Diverse alternative back-splicing and alternative splicing landscape of circular RNAs. *Genome Res* 26: 1277–1287
- Zheng X, Rui S, Wang X-F, Zou X-H, Gong Y-P, Li Z-H (2021) circPVT1 regulates medullary thyroid cancer growth and metastasis by targeting miR-455-5p to activate CXCL12/CXCR4 signaling. *J Exp Clin Cancer Res* 40: 157
- Zhong R, Chen Z, Mo T, Li Z, Zhang P (2019) Potential role of circPVT1 as a proliferative factor and treatment target in esophageal carcinoma. *Cancer Cell Int* 19: 267
- Zhu KP, Ma XL, Zhang CL (2018) Overexpressed circPVT1, a potential new circular RNA biomarker, contributes to doxorubicin and cisplatin resistance of osteosarcoma cells by regulating ABCB1. *Int J Biol Sci* 14: 321–330



License: This is an open access article under the terms of the [Creative Commons Attribution-NonCommercial-NoDerivs](https://creativecommons.org/licenses/by-nc-nd/4.0/) License, which permits use and distribution in any medium, provided the original work is properly cited, the use is non-commercial and no modifications or adaptations are made.